MEASUREMENT OF VISCOELASTIC PROPERTIES OF SOME RECENT MARINE SEDIMENTS BY A TORSIONALLY OSCILLATING CYLINDER METHOD

Steven Barker Kramer

Library
Naval Postgraduate School
Monterey, California 93940

NAVAL POSTGRADUATE SCHOOL
Monterey, California

THESIS

MEASUREMENT OF VISCOELASTIC PROPERTIES
OF SOME RECENT MARINE SEDIMENTS BY A
TORSIONALLY OSCILLATING CYLINDER METHOD

by

Steven Barker Kramer

Thesis Advisor: R. S. Andrews

September 1973

T156434

Approved for public release; distribution unlimited.

Measurement of Viscoelastic Properties of Some Recent Marine Sediments by a Torsionally Oscillating Cylinder Method

by

Steven Barker Kramer
Lieutenant, United States Navy
B.S., United States Naval Academy, 1967

Submitted in partial fulfillment of the
requirements for the degree of

MASTER OF SCIENCE IN OCEANOGRAPHY

from the

NAVAL POSTGRADUATE SCHOOL
September 1973

Library
Naval Postgraduate School
Monterey, California 93940

ABSTRACT

A torsionally oscillating cylindrical probe method, operating in the frequency range of 0.8 to 3.3 kHz was employed for measuring the visco-elastic properties of 13 marine samples collected by Shipek grab from shallow water regions of Monterey Bay, California. Other mass physical properties such as wet density, porosity, sound speed, sand-silt-clay-gravel percentages, mean grain size and sorting were also measured. Limited precision of impedance measurements permitted only the determination of the mechanical resistance due to the probe contact with the sediment. The observed values for various sediments ranged up to a value 65 times the lowest value. Correlations between mechanical resistance and mass physical properties are studied by graphical means with results indicating that water content of sediments is a determining factor in the mechanical resistance of a sediment. A dependence of mechanical resistance upon frequency is observed.

TABLE OF CONTENTS

I. INTRODUCTION ---------- 8

A. GENERAL ---------- 8

B. REVIEW OF LITERATURE ---------- 9

II. THEORY ---------- 12

III. THE VISCOELASTOMETER ---------- 15

A. DESCRIPTION ---------- 15

B. DESIGN IMPROVEMENTS ---------- 16

C. CALCULATION OF COMPLEX DYNAMIC RIGIDITY FROM EXPERIMENTAL DATA ---------- 17

IV. EXPERIMENTAL PROCEDURE ---------- 20

A. SAMPLE COLLECTION ---------- 20

B. MEASUREMENTS ---------- 20

1. Compressional Wave Speed ---------- 21

2. Complex Dynamic Rigidity ---------- 21

3. Vane Shear Test ---------- 22

4. Wet Density and Porosity ---------- 22

5. Grain Size Analysis ---------- 22

V. RESULTS ---------- 24

A. LIMITATIONS ON TORSIONAL PROBE VISCOELASTOMETER MEASUREMENTS ---------- 24

B. DISCUSSION ---------- 25

VI. CONCLUSIONS AND RECOMMENDATIONS ---------- 30

REFERENCES CITED ---------- 79

INITIAL DISTRIBUTION LIST ---------- 81

FORM DD 1473 ---------- 83

LIST OF TABLES

I. Station Location, Water Depth and Bottom Water Temperature---- 38

II. Measured Torsional Impedance of Sediments ---------- 39

III. Measured Torsional Impedance of Sediments Under Dry Conditions ---------- 41

IV. Measured Torsional Impedance of Sediments Under Mixed Conditions ---------- 42

V. Mass Physical Properties of Sediments ---------- 43

VI. Acoustic Properties of Sediments ---------- 44

VII. Textural Analysis of Sediments ---------- 45

LIST OF FIGURES

1. Sketch of the Viscoelastometer ---------- 32

2. Sketch of the Piezoelectric Ceramic ---------- 33

3. Sketch of the Velocity Sensor ---------- 34

4. Sketch of the Vaned Head ---------- 35

5. Diagram of Electronics for Experimental Measurements --------- 36

6. Shepard Tertiary Sediment Type Diagram ---------- 37

7. R_L as a Function of Wet Density, First Mode ---------- 46

8. R_L as a Function of Wet Density, Second Mode ---------- 47

9. R_L as a Function of Wet Density, Third Mode ---------- 48

10. R_L as a Function of Porosity, First Mode ---------- 49

11. R_L as a Function of Porosity, Second Mode ---------- 50

12. R_L as a Function of Porosity, Third Mode ---------- 51

13. R_L as a Function of Sound Speed, First Mode ---------- 52

14. R_L as a Function of Sound Speed, Second Mode ---------- 53

15. R_L as a Function of Sound Speed, Third Mode ---------- 54

16. R_L as a Function of the Product of Wet Density and Sound Speed Squared, First Mode ---------- 55

17. R_L as a Function of the Product of Wet Density and Sound Speed Squared, Second Mode ---------- 56

18. R_L as a Function of the Product of Wet Density and Sound Speed Squared, Third Mode ---------- 57

19. R_L as a Function of Percent Sand, First Mode ---------- 58

20. R_L as a Function of Percent Sand, Second Mode ---------- 59

21. R_L as a Function of Percent Sand, Third Mode ---------- 60

22. R_L as a Function of Percent Silt, First Mode ---------- 61

23. R_L as a Function of Percent Silt, Second Mode ---------- 62
24. R_L as a Function of Percent Silt, Third Mode ---------- 63
25. R_L as a Function of Percent Clay, First Mode ---------- 64
26. R_L as a Function of Percent Clay, Second Mode ---------- 65
27. R_L as a Function of Percent Clay, Third Mode ---------- 66
28. R_L as a Function of Percent Gravel, First Mode ---------- 67
29. R_L as a Function of Percent Gravel, Second Mode ---------- 68
30. R_L as a Function of Percent Gravel, Third Mode ---------- 69
31. R_L as a Function of Vane Shear Strength, First Mode ---------- 70
32. R_L as a Function of Vane Shear Strength, Second Mode ---------- 71
33. R_L as a Function of Vane Shear Strength, Third Mode ---------- 72
34. R_L as a Function of Mean Grain Size, First Mode ---------- 73
35. R_L as a Function of Mean Grain Size, Second Mode ---------- 74
36. R_L as a Function of Mean Grain Size, Third Mode ---------- 75
37. R_L as a Function of Sorting, First Mode ---------- 76
38. R_L as a Function of Sorting, Second Mode ---------- 77
39. R_L as a Function of Sorting, Third Mode ---------- 78

ACKNOWLEDGEMENTS

The author wishes to express his gratitude to Professors O.B. Wilson, Jr., and R.S. Andrews for their assistance in this research. The author also wishes to thank Physicist Donald E. Spiel for his valuable assistance.

Use of the R/V ACANIA, operated by the Naval Postgraduate School, was essential in this research as was project support received through contract with the Office of Naval Research, Ocean Sciences and Technology Division. The sediment velocimeter used in the research was provided by the Navy Pacific Support Group of the Naval Oceanographic Office, San Diego, California.

I. INTRODUCTION

A. GENERAL

A better understanding of the transmission and loss of acoustic energy in marine sediments is needed in order to improve the usefulness of sound reflection from the ocean bottom. Geologists conducting seismic research or seismic prospecting are interested in better understanding how acoustic energy is transmitted and attenuated in the ocean floor. The acoustician may be interested in improving the accuracy of sonic profiling, precision acoustic mapping, and the sonic probe. The Naval officer may desire a better understanding of the effect of the bottom upon long range propagation and more reliable predictions of ocean areas where bottom bounce mode sonar has maximum effectiveness. Refinements in all of these uses of reflected acoustic energy may ultimately depend upon how accurately energy losses at the ocean floor can be predicted.

A major difficulty in making energy loss predictions is due to the variability of marine sediments and in applying a model that describes this variability. Variability may be the result of both vertical inhomogenities due to layering or horizontal inhomogenities caused by changes in sedimentation, situations which are common in ocean sediments. Another problem is that of developing a reflection process model which incorporates more realistic values of the physical properties of the sea floor.

When a compressional wave strikes the bottom, some of its energy is reflected and some penetrates causing energy losses due to attenuation

and to transformation into shear waves and the propagation of the shear waves in the sediment (Hamilton et al.,1970). The energy losses from these effects were omitted from some of the earlier models which were used for bottom loss predictions. The near elastic model, or viscoelastic model, is one of the more sophisticated models in current use which accounts for these energy losses. In this model, Lamé constants in the Hookean equations of elasticity are replaced with complex Lamé constants whose real part represents elastic activity and whose imaginary part represents damping of compressional acoustic wave energy or energy losses due to friction (Hamilton, 1969). Researchers have hoped that the viscoelastic model would provide accurate reflection coefficients, but comparisons between experimental results and theoretical calculations have had mixed success (Bucker et al., 1965; Akal, 1972). There exist problems in determining values of the viscoelastic parameters for use in acoustic reflection modeling.

B. REVIEW OF LITERATURE

Investigators have attempted to measure complex Lamé constants by four different methods. The Stoneley wave technique has been used by Hamilton et al. (1970) and Bucker, Whitney, and Keir (1964) and the torsional wave vibration technique has been described by Gallagher (1968). Another method, the direct measurement of shear wave speed in sedimentary rocks, was noted by White (1965). The torsionally oscillating cylinder method was developed by Mason (1947) and McSkimin (1952) for use in polymer research.

At the Naval Postgraduate School (NPS), investigators have studied various designs of a viscoelastometer utilizing the torsionally oscillating cylinder method in an attempt to directly measure one of the complex Lamé constants, the complex dynamic rigidity. Hutchins (1967) used a torsional

wave viscoelastometer in the frequency range near 38.8 kH_z to measure the complex shear modulus (complex dynamic rigidity) in a kaolinite-water mixture which simulated an ocean sediment. Cohen (1968) extended the frequency range of Hutchins' viscoelastometer, and studied a kaolinite-bentonite-water artificial sediment and showed that this mixture exhibited shear moduli independent of frequency. The complex dynamic rigidity of some shallow water marine sediments was measured by Bieda (1970) and correlated with mass-physical properties of these sediments. Lasswell (1970) attempted to verify the rigidity values of Beida by another method and found them to be in close agreement. Walsh (1971) also attempted to verify the viscoelastic measurements of complex dynamic rigidity of previous investigators. Using kaolinite and water as a model for the ocean bottom, shear wave speeds were found to be similar to those calculated from previously measured values of rigidity. A newly designed viscoelastometer was used by Engel (1973) when measuring rigidity of shallow water clayey silt marine sediments. Results of these studies showed trends between complex dynamic rigidity and mass-physical properties of the sediments which were in agreement with other investigators. The instrument used by Engel was originally intended for in situ use but it was found to be too sensitive to temperature. In an effort to overcome temperature dependence and to provide an in situ capability, Morgan (1972) designed and constructed a basic version of a vaned torsionally oscillating cylinder type of viscoelastometer. Improvement of this design was carried out in early 1973 by Physicist Donald E. Spiel of NPS. This instrument was used in the measurements reported here.

The purpose of this research is to measure the complex dynamic rigidity of marine sediments with a newly designed torsional wave viscoelastometer and to correlate measurements with mass physical properties. The following

sections describe the operation and design of the viscoelastometer, the theory of measurement, and experimental procedure. Following these sections, a discussion of results and recommendations for future research are presented.

II. THEORY

The torsional oscillation of a cylinder embedded in a sediment will generate shear waves which propagate into the sediment. This type of instrument system, called a viscoelastometer, measures the mechanical impedance due to the radiation reaction from the shear waves using torque and angular velocity sensors located in the cylindrical probe. The mechanical impedance can be related to the real and imaginary components of the complex dynamic rigidity modulus for the medium. The Voigt model of a viscoelastic solid is convenient for the specification of these components. A development of this model is presented by Ferry (1970).

McSkimin (1952) developed a relationship between the components of the dynamic rigidity modulus and the mechanical radiation impedance presented by contact with the walls of a cylinder executing simple harmonic motion.

If the specific impedance for the generated shear waves is given by:

$$Z_o = R_o + jX_o, \tag{1}$$

where R_o and X_o are the specific resistance and reactance, respectively, then the real and imaginary components of the dynamic rigidity modulus, $G = G_1 + jG_2$ (Voigt model) are given by:

$$G_1 = \frac{R_o^2 - X_o^2}{\rho_{sed}} \quad \text{and} \quad G_2 = \frac{2R_oX_o}{\rho_{sed}} \,. \tag{2}$$

The term ρ_{sed} is the wet density of the medium. A relationship between the measured torsional impedance due to contact with the sediment, Z_L, and the specific impedance of shear waves, Z_o, is found by first defining torsional impedance as:

$$Z_L = \frac{T}{\Omega} \,, \tag{3}$$

where T and Ω are the applied torque and angular velocity of the cylinder, respectively. The cylinder of length L and radius a is assumed to be oscillating in pure torsional simple harmonic motion without slip at the cylinder-sediment boundary. The wavelength of the shear waves generated is assumed to be very small compared to the dimensions of the cylinder and it is assumed the wave is rapidly attenuated. In this case, the torsional impedance and the specific impedance for the shear waves is given by:

$$Z_L = BZ_o \quad . \tag{4}$$

It is shown below that:

$$B = 2\pi a^3 L_o \quad . \tag{5}$$

The area of the cylinder in contact with the sediment is $2\pi aL$. The shear mechanical impedance presented to the cylinder by the shear waves is:

$$Z_m = 2\pi aLZ_o = \frac{\text{Force}}{\text{Velocity}} = \frac{F}{v} \quad , \tag{6}$$

where v is the velocity associated with the shearing motion at the wall of the cylinder and F is the shearing force exerted on the sediment. Therefore:

$$F = 2\pi aLZ_o v \quad . \tag{7}$$

The torque thus defined is:

$$T = Fa \quad . \tag{8}$$

Substituting equation (7) for F gives:

$$T = 2\pi a^2 LZ_o v \quad . \tag{9}$$

Using the relationship $\Omega = v/a$, equation (3) becomes:

$$Z_L = \frac{2\pi a^2 LZ_o v}{\Omega} = 2\pi a^3 LZ_o = BZ_o \quad . \tag{10}$$

For the instrument used in this research, B is equal to 85 cm^3, giving the specific mechanical impedance of the sediment as:

$$Z_o = \frac{Z_L}{85} = R_o + jX_o \ , \qquad (11)$$

where:

$$R_o = \frac{R_L}{85} \text{ and } X_o = \frac{X_L}{85} \ . \qquad (12)\ (13)$$

Substitution of these quantities into equation (2) provides the real and imaginary parts of complex dynamic rigidity.

III. THE VISCOELASTOMETER

The viscoelastometer used in the data collection for this report was originally designed by Morgan (1972), but it has been modified as described below.

A. DESCRIPTION

While the probe is operating at mechanical resonance, the shaft and the vaned head are driven together in torsion by the piezoelectric barium titanate transducer located below the support flange (Fig. 1). With the vaned head (Fig. 4) submerged in a sediment, shear waves are generated and propagated radially outward from the head as the viscoelastometer executes torsional simple harmonic motion. The radiation of shear waves has a loading effect on the mechanical system as described above and the piezoelectric barium titanate ceramic torque sensor produces a voltage proportional to the torque loading (Fig. 2). This voltage is increased by a preamplifier and its magnitude is read from a voltmeter. The angular velocity sensor inside the steel tube and probe head produces a voltage proportional to the angular velocity of the head as the coil oscillates around the essentially stationary permanent magnet (Fig. 3). This voltage is amplified by a preamplifier and read from a voltmeter. The phase difference between the torque voltage and the velocity voltage is read from the phase meter. The frequency of the oscillation is measured from the frequency counter (Fig. 5) connected to the drive oscillator. Normally, the system is operated at a frequency which gives torsional resonance and a concomitant increase in amplitude of motion. Drive levels are adjusted to give an adequate signal to noise ratio in the sensor outputs.

B. DESIGN IMPROVEMENTS

Improvements have been made in a number of details of the viscoelastometer described by Morgan (1972) although the basic principles of operation were retained (Fig. 1). The technique for cementing the barium titanate ceramics to the stainless steel tubing was improved. The ends of the ceramics were carefully notched and the steel tubing ends facing these notched ends were drilled with several holes to a diameter and depth of 1/16 inch (2.46 mm). This was done to increase the shear strength of the ceramic-steel bond. The position of electrical leads from the ceramic was changed from the middle of the ceramic to the end to facilitate electrical connection. Integrated circuit preamplifiers were constructed and located inside the probe tube. The preamplifiers for the velocity sensor and the torque sensor were designed for a gain of 400 and 0.05, respectively. The velocity sensor coil was rewound with No. 44 gauge wire to produce a 280 ohm coil and the permanent magnet was suspended by No. 30 spring bronze wire. These changes increased the sensitivity of the velocity sensor. The coil and permanent magnet assembly were placed inside a mild steel cylinder. Figure 2 shows a sketch of this cylinder with the assembly inside.

The vaned head used in this research was constructed of aluminum and is illustrated with dimensions in Figure 3. Substituting aluminum for stainless steel reduced the mass of the head from 40.9 to 13.6 g which allowed the moment of inertia of the head to be much smaller and thus increased the sensitivity of the instrument. The support handles interfered with calibration and were replaced with a spring steel support wire. The details of the electrical cables were modified. The length of the three RG 58C/U coaxial cables connecting these leads with the various meters was increased from the length of approximately 3 m to 152.5 m.

This additional length was needed for in situ work. The integrated circuit preamplifiers and more sensitive angular velocity sensor improved signal to noise ratio considerably so that the voltage amplifier and filter, used previously, were not needed. A frequency meter was added to the transducer circuit. The circuitry used in this experiment is illustrated by a block diagram in Fig. 5. The models of the equipment are as follows: three Hewlett Packard Model 400L voltmeters, a Dranetz 305-PA-3002 phase meter, a Tektronix Model 555 oscilloscope, a General Radio Model 1309A oscillator, a Krohn-Hite Model DCA-50B power amplifier, and a General Radio 1192B frequency counter.

C. CALCULATION OF COMPLEX DYNAMIC RIGIDITY FROM EXPERIMENTAL DATA

The torsional mechanical impedance for the oscillating cylindrical probe is the ratio of torque, T, to angular velocity, Ω, expressed in equation (3). It is measured using torque and angular velocity sensors which provide voltages v_T and v_V, respectively, proportional to these mechanical quantities. If K is the proportionality between the electrical and mechanical values, then:

$$Z = |K| \left| \frac{v_T}{v_V} \right| e^{j\theta} , \qquad (14)$$

where K is determined by calibration of the torque and velocity sensors as described by Andrews and Wilson (1973). Masses of known moments of inertia are attached to the probe when it is vibrating in air, where it is assumed that the torsional impedance is purely reactive and consists of the inertia of the probe itself and the added mass. Using a series of masses of known moment of inertia, a value for K can be determined. The term θ is determined from the observed phase angle, θ_o, between torque

and velocity voltages when the instrument is embedded in the sediment. The phase angle correction, due to phase shifts in the preamplifiers, is made by the equation:

$$\theta = \theta_o - \theta^* , \tag{15}$$

where θ^* is determined by:

$$\theta^* = \theta' - 90^o , \tag{16}$$

where θ' is the phase angle between the torque and velocity voltages when the instrument is unloaded or in air.

The calculation of specific mechanical impedance follows the development presented by Andrews and Wilson (1973). Torsional impedance Z defined in equation (14) has two parts:

$$Z = Z_H + Z_L , \tag{17}$$

where Z_H is the impedance due to the inertia of the cylindrical probe alone and Z_L is the impedance due to the load applied to the probe by the sediment (equation 3). The value for Z_H in equation (17) is calculated by:

$$Z_H = j\,\omega I_H , \tag{18}$$

where I_H, the moment of inertia of the probe alone, is determined from measurements of impedance Z made in air where $Z_L = 0$. The torsional mechanical impedance, Z_L, due to contact of the probe with the sediment has both real and imaginary parts:

$$Z_L = R_L + jX_L . \tag{19}$$

The term R_L is the mechanical or radiation resistance of the load on the probe and is found by the equation:

$$R_L = Z\cos\theta . \tag{20}$$

The mechanical reactance X_L of the load is found from the relation:

$$X_L = Z\sin\theta - Z_H \ , \tag{21}$$

where Z is determined by equation (14). Calculating the specific mechanical resistance and reactance by equations (12) and (13), respectively, and substituting these quantities into equation (2) gives the complex dynamic rigidity of the sediment.

IV. EXPERIMENTAL PROCEDURE

A. SAMPLE COLLECTION

Thirteen samples of marine sediment were collected from Monterey Bay, California, at depths up to 85 fathoms (155.4 m) (Table I). From the time of collection until laboratory measurements were completed, a great deal of care was exercised to keep the samples as undisturbed as possible or conditions as near to those in situ as possible. A Shipek grab sampler, selected to collect samples, provided sample dimensions large enough in area and depth to allow several insertions of measuring instruments into different locations in a given sample. The large dimensions of the sample bucket also helped to reduce the wall effects on the measurements taken with the viscoelastometer and the vane shear machine.

When the sample was brought aboard the research vessel (NPS R/V ACANIA), the bucket was carefully removed and placed in a wood rack which provided stability for the sample. The samples were kept submerged in sea water, sealed in plastic bags and stored in the ship's refrigerator. The samples remained covered with sea water in their original containers and refrigerated throughout the experiment in order to approximate in situ conditions.

B. MEASUREMENTS

The measurements for each sample were conducted in a standard sequence so that a previous measurement would cause a minimal disturbance in the sample for the next measurement. The sequence of measurement was as follows: compressional wave speed, torsional probe measurements, vane shear test, and wet density and porosity. Finally, grain size analysis was performed on the samples.

1. Compressional Wave Speed

The first test on the samples was compressional wave speed measurement. The Underwater Systems, Inc., Velocimeter Model USI 101 was used to measure the time delay between a transducer and receiver submerged at a fixed distance into opposite sides of the sediment in the sampler bucket. The bracket fixing the distance between the transducer and receiver did not penetrate more than a few millimeters into the surface of the sediment: therefore, the sample between the receiver and transducer was essentially undisturbed. The arrival time of the signal was read from the oscilloscope of the velocimeter and the temperature of the sediment was recorded using a United Systems Corp. Digital Thermometer. Later, the time delay in sea water was measured at the same temperature at which time delay measurements were made in the samples, and thus a temperature correction was unnecessary.

2. Complex Dynamic Rigidity

The next step was to conduct measurements with the torsional probe. Before insertion of the probe in the sediment, certain measurements were made while the instrument was in the unloaded condition (i.e., suspended in air). The following data were always recorded at a drive voltage of 3 v: frequency of mechanical resonance at three modes, torque sensor and velocity sensor voltages at each resonant mode, and the corresponding phase angle between the two voltages. The sample, still in its original container and saturated with water was placed under the viscoelastometer and the vaned head was lowered carefully into the sediment. The depth of penetration was recorded and the drive voltage was increased to 15 v. A waiting period was established until the temperature of the probe reached the temperature of the sample. This temperature was then recorded and the same data were recorded as in the unloaded condition and at resonant

frequencies of about 0.8 kHz, 2.2 kHz, and 3.1 kHz. Depth of penetration was varied in some samples and in others there were several insertions of the vaned head at different locations.

3. Vane Shear Test

The third step was the use of the Wykeham-Ferrance Engineering Ltd. Vane Shear Machine which had the Diversified Marine Corporation Laboratory Vane Shear Transducer and Adapter Kit Model LVST-015 attached. This adapter kit is fully described by Cepek (1972). The constant speed drive motor which is also a modification allows an X-Y plotter to trace a curve of torque versus angle of rotation as the vane rotates in the sediment at a rate of 20^{o}/min.

The samples, still in their original containers, were placed under the vane so that it would penetrate an undisturbed region of the sediment.

4. Wet Density and Porosity

The last measurements taken which could be affected by disturbing the sediment were wet density and porosity. These were calculated for each sample by filling two stainless steel cylinders of known volume with sediment and then weighing them on an electric chemical balance. The samples were then oven dried for 24 hours at 105 C and, after cooling in a dessicator to prevent absorption of moisture, were reweighed. Two densities and porosities were then calculated and averaged for each sample.

5. Grain Size Analysis

Analysis of the grain size distribution was also carried out for each sample. A portion of each sample was washed thoroughly by first mixing with water in an electric blender and then washing into a jar where settling took place. After settling, water was carefully decanted and tap water was added again for a second washing. After setting again,

water was decanted from the sediment and the sediment was washed through a 4Ø (0.062 mm) sieve. The fraction of the sample with grain sizes coarser than 4Ø (sand and gravel) was oven dried and size analysis was performed by sieving. The distribution of grain sizes finer than 4Ø (silt and clay) was determined by pipette analysis.

V. RESULTS

A. LIMITATIONS ON TORSIONAL PROBE VISCOELASTOMETER MEASUREMENTS

The calibration of torque and angular velocity sensors and the accuracy of all measurements permit a precision of about 5% or 6% in the calculated components of torsional impedance presented to them. The real part of this impedance, the mechanical resistance, R_L, which is due only to contact with the sediment is thus precise to within about 5%. The imaginary part of this impedance, which can be measured to within about 6%, is dominated by the inertia of the probe. In many cases, the contribution to the reactance from the sediment is comparable to the uncertainty in the total reactance. Therefore when equation (21) is used to calculate X_L, a large uncertainty in X_L may occur. As a result, values of X_L are not precise enough to justify calculation of both the real and imaginary parts of complex dynamic rigidity. Therefore, values of rigidity are not presented as had originally been intended. Since R_L is sensitive to both the elastic (G_1) and the anelastic (G_2) properties of the sediment, it is a measure of the viscoelastic properties of the sediment. As a result of this sensitivity it is useful to test correlations between values of R_L with other measured properties of each sediment. This may be done using graphical methods.

If X_L could be considered as small and insignificant, then G_1 is approximately proportional to R_L^2 and a comparison between the relation of R_L and other properties from this experiment and similar relationships for the real part of dynamic rigidity obtained by other investigators may be useful.

Measurements of R_L were conducted at three different frequencies so that the relative size of the probe (in terms of wave length) are different in each case. This will change the coupling to the medium and therefore

will give rise to a sensitivity of radiation or mechanical resistance to frequency. The computation of this effect could not be completed. This leaves uncertain whether frequency dependence in R_L is due to a change in basic viscoelastic properties with frequency or merely to a change in the coupling between the probe and the medium.

An important limitation to the conclusions that may be drawn from the graphs presented is the small sample size used in this experiment. Thirteen separate samples were analyzed and twenty-three viscoelastometer measurements were performed. A larger sample size would give more credibility to apparent trends.

B. DISCUSSION

Most of the values of mechanical resistance and reactance measured with the viscoelastometer are presented in Table II. Also included in this table are the frequency at which each measurement was made, the depth of penetration of the vaned head into the sediment, and the wet density of each sediment. In many of the sediments several measurements were taken with the viscoelastometer (these data are indicated by small case letters accompanying the large case letter and number, the latter identifying the original sediment sample). Values of R_L range from 0.88×10^4 to 32×10^4 g-cm^2/sec, frequency of measurement ranges from 0.87 to 3.3 kHz, and depth of penetration ranges from 4.49 to 7.49 cm. The data in this table represent measurements conducted under conditions of minimum sample disturbance, saturated sediments, and with all samples at nearly the same temperature.

In several cases, there are large differences in the values of R_L measured in different regions of the sample. This variability is apparently caused by horizontal and vertical inhomogenities which exist in the sediments. Some of these inhomogenities were readily apparent, for example, the existence of biological forms and or pieces of gravel near the measuring

site. The amount of disturbance to which the samples were subjected is uncertain. It is impossible to determine, in each case, whether the value of R_L at a particular site in the sample was the result of the effects of collection, handling, and/or temperature variation upon the structure of the sediment.

Table III lists the same kinds of data presented in Table II but measured under different laboratory conditions. These measurements were conducted near the edge of three of the samples where the sediment was somewhat elevated and therefore partially drained. As expected, the measured mechanical resistance in these regions was in general larger at all frequencies than most values recorded for the submerged portions of the sediments. These values of R_L range from 13×10^4 to 28×10^4 g-cm^2/sec.

Measurements with the viscoelastometer were repeated in each W-series sediment sample (Table I) after it was thoroughly stirred and the remolded sample placed into a cylindrical container. These data are presented in Table IV. The range of values for radiation resistance in these nearly homogeneous sediments is 0.49×10^4 to 4.1×10^4 g-cm^2/sec. These values are in general lower than those observed in the "undisturbed" and saturated sediments in Table II and are also smaller than values measured for the dryer sediments listed in Table III. The values of R_L are lower since any cementation or compaction existing in the samples was destroyed by remolding. The differences in R_L between the individual "homogeneous" samples is not nearly as large as differences in R_L between the various "undisturbed" samples. This may indicate that the viscoelastometer is indeed responding to properties of the sediment such as structure, rigidity, and water content.

Values of R_L listed in Table II are used as the dependent variable in all of the graphs presented. The independent variables are as follows: wet density, porosity, compressional wave speed, the product of the square of compressional wave speed and the wet density, percent sand, percent silt, percent clay, percent gravel, vane shear strength, mean grain size, and grain size distribution standard deviation (sorting). Values of R_L are compared with each of these independent variables at each of the three frequencies of mechanical resonance, about 0.87, 2.2 and 3.3 kHz for the first, second and third modes, respectively.

The comparison of mechanical resistance with density (Fig. 7, 8 and 9) exhibits a general increase in resistance of the sediment with increasing density, particularly in the second mode. The results obtained by Hamilton (1969), Beida (1970), and Engel (1972) indicated an increase in dynamic rigidity with increasing density. Rigidity is lower in sediments with high porosity (lower density) since there are fewer interparticle contacts due to the presence of water between the particles (Hamilton,1969). An increase in R_L with decreasing porosity is observed in all three modes (Fig. 10, 11 and 12).

The measured compressional wave speeds in the different types of sediments used in this experiment are distributed over a moderate range. Mechanical resistance appears to show a fairly strong trend with sound speed, increasing as the sound speed decreases (Fig. 13, 14 and 15). An increase in sound speed with an increase in rigidity (or mechanical resistance of the sediment) might be expected since with increased rigidity there are probably more particles in contact which should also affect the compressive modulus. Beida (1970) did not show such a relationship between the dynamic rigidity and sound speed.

Data, including the ratio of the speed of sound in a sediment to the compressional wave speed in water, the in situ compressional wave speed, and ρC^2 are presented in Table VI. A comparison between the R_L and ρC^2 shows no apparent trends (Fig. 16, 17 and 18). However, Engel (1973) found trends between the real part of dynamic rigidity and ρC^2 which showed a slight increase in rigidity with an increase in ρC^2. This was in agreement with Hamilton (1969) and Beida (1970).

The types of sediments considered in this research are different from those studied by Engel (1973) which were primarily clay and silty clay types. Most of the sediments analyzed in this experiment are the silt and sandy silt types with one sample of the silty sand type and two other sand types (Fig. 6). One sand type sample contained a large percentage of gravel (Table VII). The depositional environment of the sediments collected for this experiment is also different than those of other investigators. Sediments presently under consideration were collected from shallow water (Table I) and most other researchers obtained sediments from much deeper locations where the rates of deposition and compaction are slower. The differences of sediment type and depositional environment may account for some of the apparent disparities in trends between results reported here and those of other investigators.

A comparison of R_L with the percent of sand indicates an increase in R_L with an increase in percent sand for all three frequencies of resonance (Fig. 19, 20 and 21). The resistance might be expected to increase due to the friction from more particles of sand in sediments of higher percentages of sand. An inverse relationship is observed in a comparison of R_L to the percent silt where R_L increases as the percent silt decreased. This again may be a clue to the presence of water between adjacent particles reducing resistance to movement (Fig. 22, 23 and 24). Only the

first and second modes show a slight trend with R_L which increases as percent clay decreases (Fig. 25, 26 and 27). The comparison of R_L with percent gravel shows an increase in mechanical resistance with an increase in percent gravel (Fig. 28, 29 and 30) perhaps due to less water between particles.

Vane shear strength reported by Engle (1973) and Beida (1970) indicated a slight increase in vane shear strength with rigidity. A similar result is observed in the comparison between R_L and vane shear strength in Fig. 31, 32 and 33, although it is not a strong dependence.

Mean grain size and sorting (deviation) presented in Table VII are compared with R_L. Values of R_L increase as the mean grain size and sorting increase (Fig. 34 through 39). This result is in agreement with the behavior of R_L when compared with percent sand, silt, clay, and gravel. Greater amounts of larger grain sizes in these comparisons show an increase in R_L. It is also noted that, as would be expected, porosity tends to decrease with increasing standard deviation (i.e., poorer sorting).

In general, the values of R_L exhibit a frequency dependence. At the first mode (lowest frequency), values of R_L are relatively lower, particularly in the range of the smaller values, than in the second (intermediate frequency) and third modes (highest frequency). Second mode R_L values are larger than first mode values of R_L and third mode values are the largest. This pattern, with a few exceptions, is observable in each graph presented. Neither Beida (1970) nor Engle (1973) found this dependence when analyzing complex dynamic rigidity with independent variables similar to those reported here. For the reasons discussed in Part A of Chapter V, it is not possible to draw conclusions from this pattern of frequency dependence.

VI. CONCLUSIONS AND RECOMMENDATIONS

It is concluded that the present configuration of the torsional wave viscoelastometer fails to measure mechanical reactance of the sediment with the precision necessary to calculate useful values of real and imaginary dynamic rigidity. However, relationships between measured values of mechanical resistance and other mass physical properties compare favorably in most instances with results achieved by previous investigators at the Naval Postgraduate School as well as at other institutions.

Summarizing the results, it can be said that sediments which were maintained in a saturated and undisturbed condition provide values of mechanical resistance which vary between each sample and at different regions in a sample. Remolded sediments exhibit the lowest values of mechanical resistance and the smallest differences in value between different samples in the experiment. Portions of sediments which were not saturated show the highest mechanical resistance. Graphical relationships between measured mechanical resistance and mass physical properties indicate that the amount of water between particles has a key role in determining the resistance of a sediment, the resistance increasing with less water present. The generally observed relationship that values of resistance increase with an increase in frequency cannot be interpreted at this time.

In the future, the re-evaluation of the assumptions made in the development of the relationship of torsional impedance to the viscoelastic model needs to be carried out. In particular, the assumption that there is no slippage at the sediment-rod interface may be invalid and needs careful consideration. Water may easily prevent the contact between the sediment and the vaned head. In the future a more sensitive torsional wave viscoelastometer should be developed which incorporates an improved design

for the torque and angular velocity sensors with a probe head that guarantees actual contact with the medium.

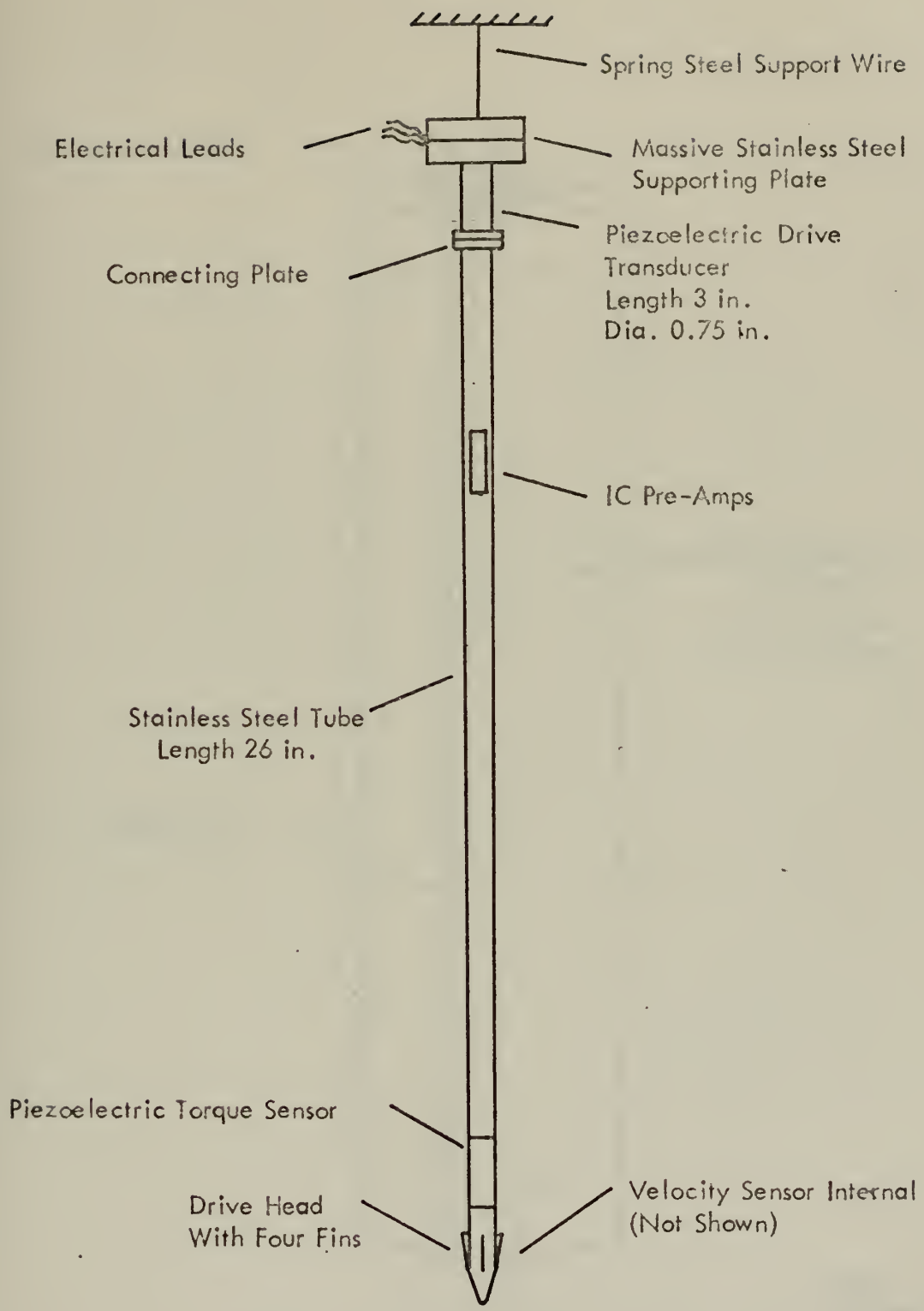

Figure 1. Sketch of the Viscoelastometer

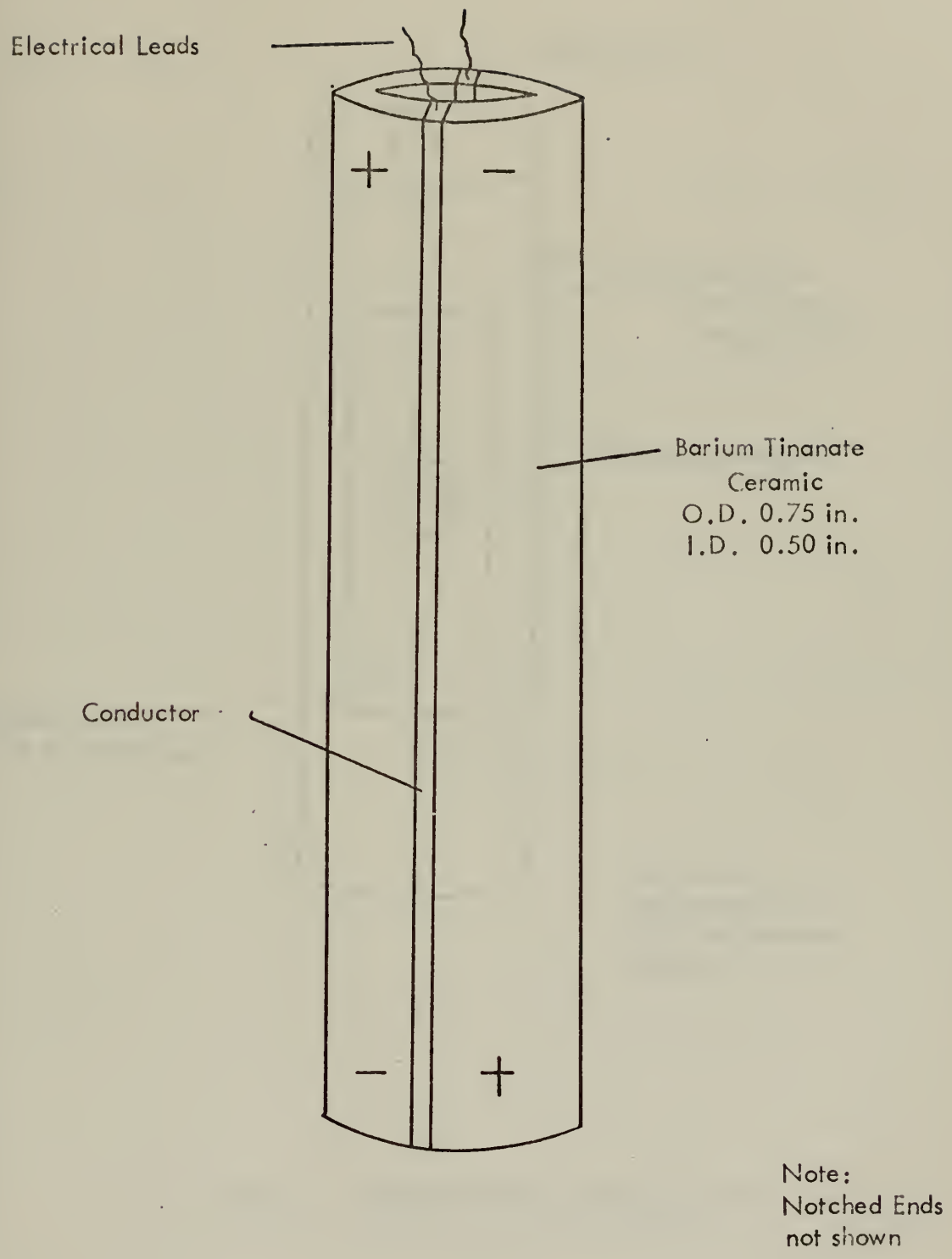

Figure 2. Sketch of the Piezoelectric Ceramic

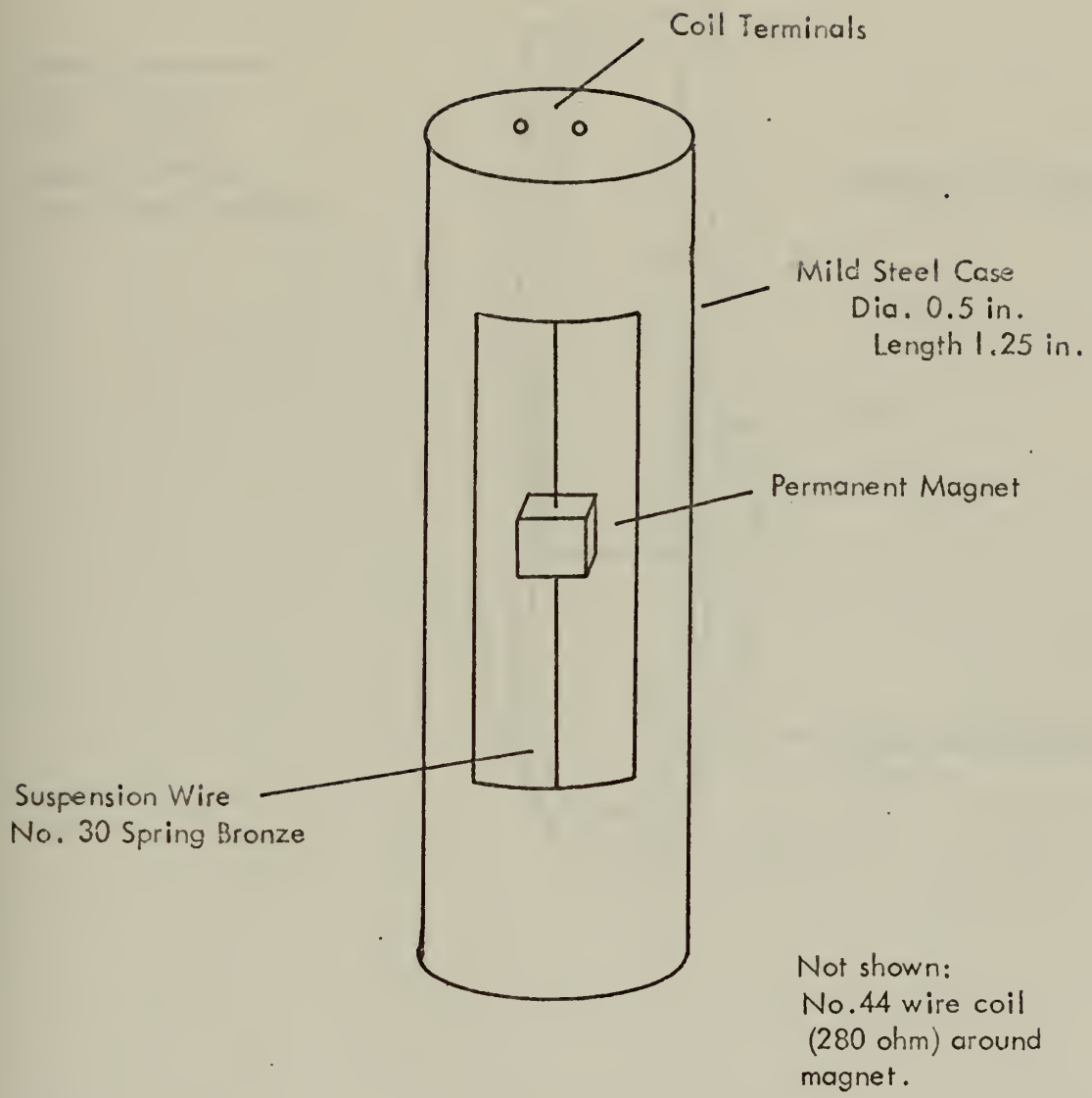

Figure 3. Sketch of the Velocity Sensor

Head Dimensions:
I. D. 1.78 cm.
O.D. 1.90 cm.
Length 4.49 cm.
Vane Width 0.062 cm.

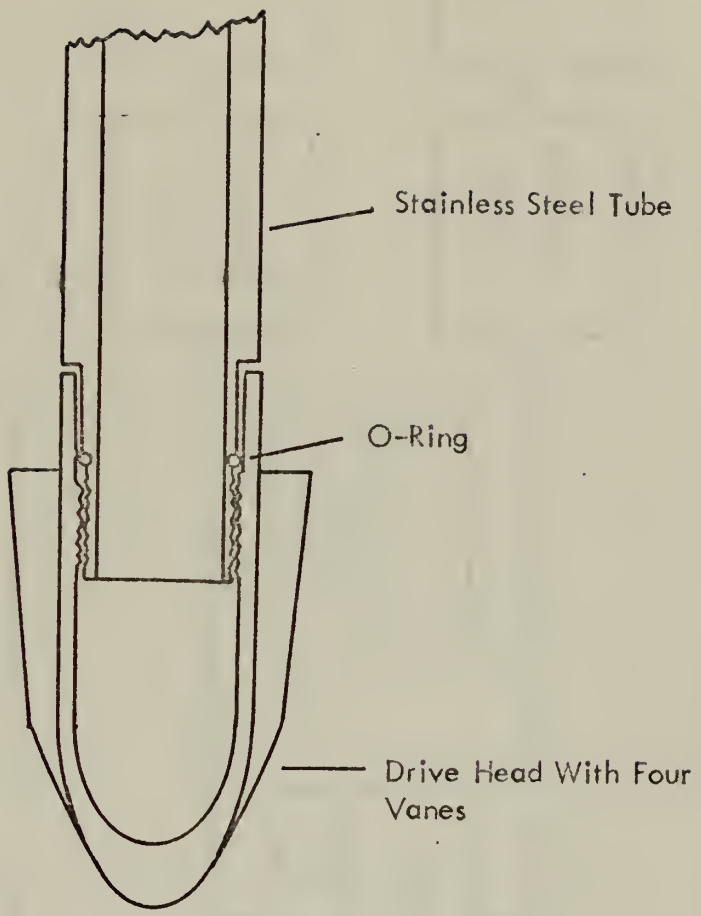

Figure 4. Sketch of the Vaned Head

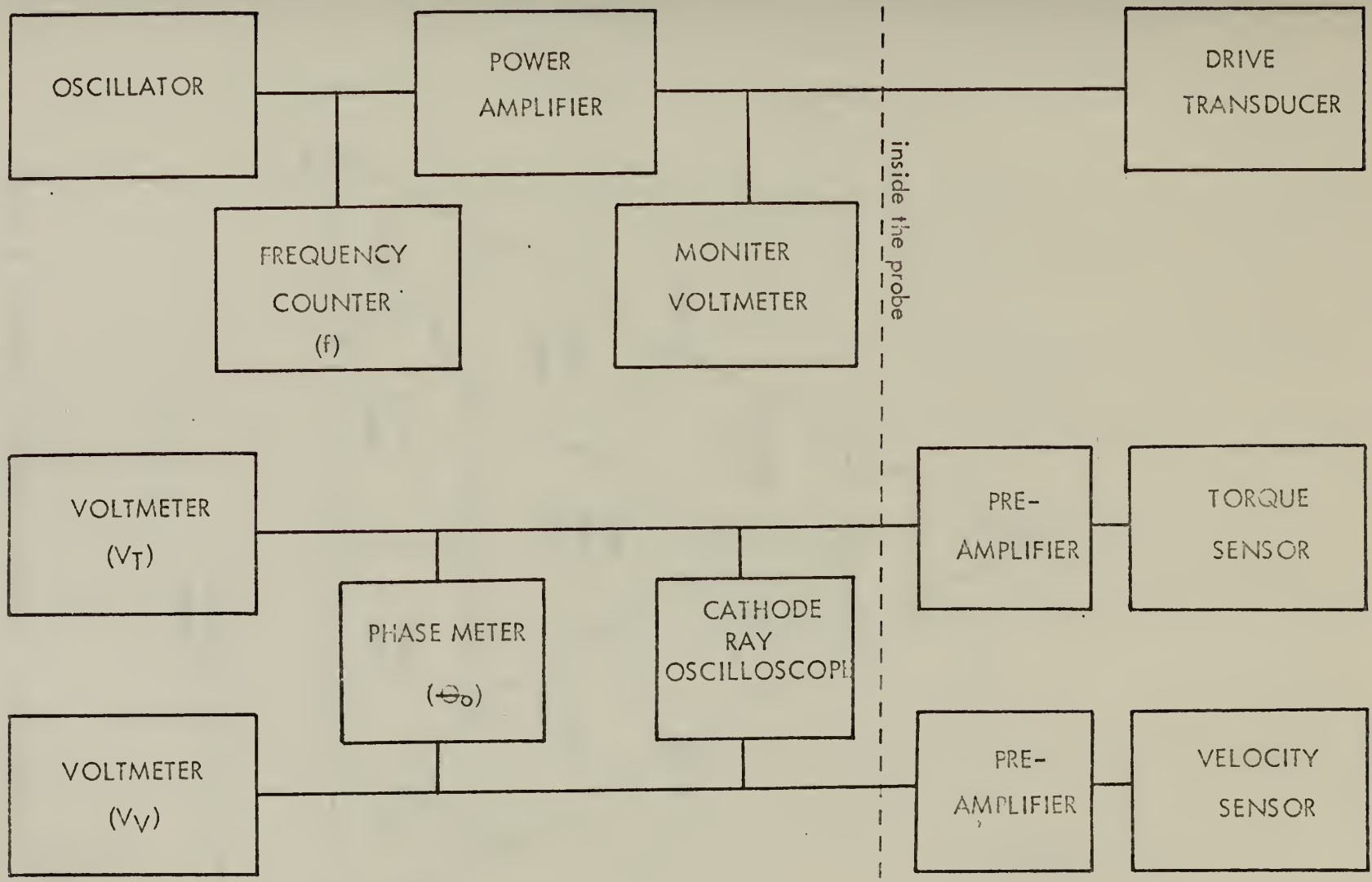

Figure 5. Diagram of Electronics for Experimental Measurements

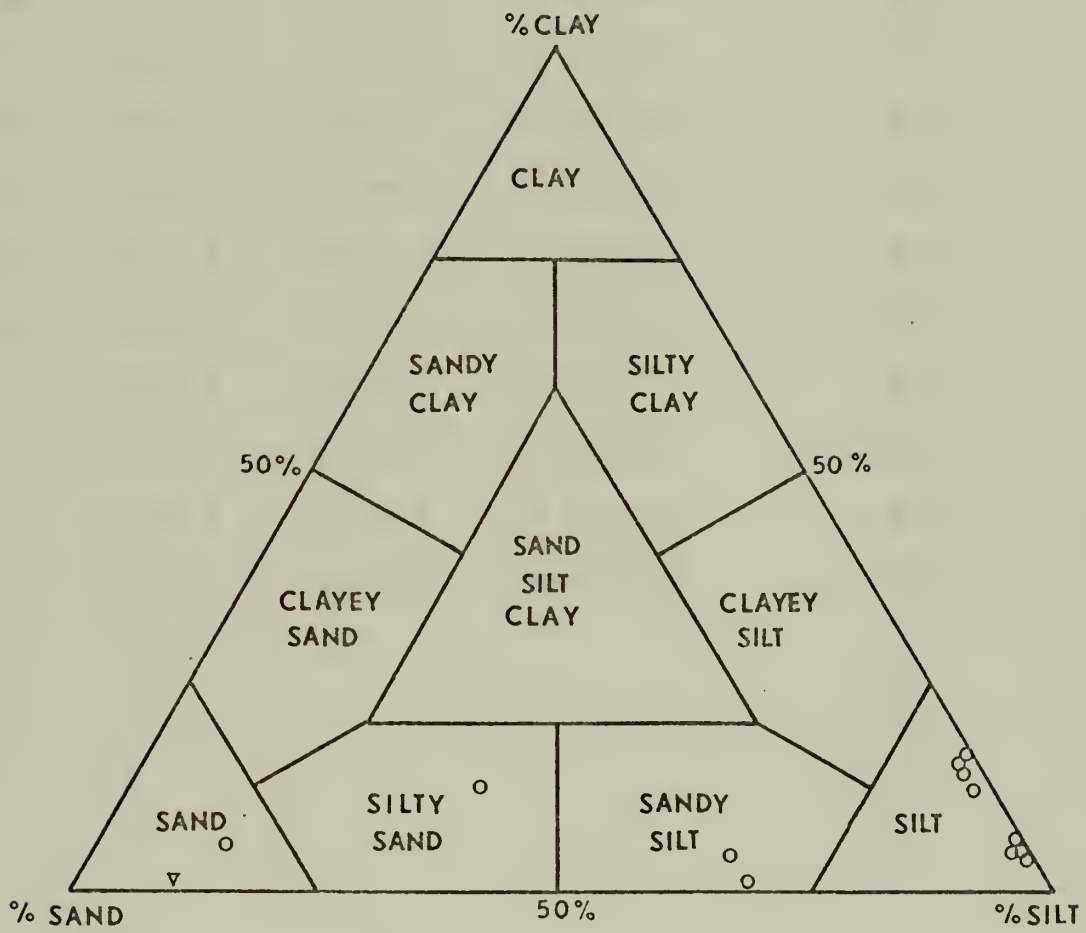

▿ This point includes percent of gravel.

Figure 6. Shepard Tertiary Sediment Type Diagram

Sample	Latitude N	Longitude W	Water Depth fm (m)	Bottom Water Temperature, °C
W-1(a,b)	36-45.2	121-56.9	54 (98.8)	8.0
W-2(a,b)	36-45.2	121-56.9	54 (98.8)	8.2
W-3(a,b)	36-44.8	121-53.2	53 (96.9)	8.2
W-4(a,b,c)	36-44.8	121-53.2	53 (96.9)	8.2
W-5(a,b)	36-41.6	121-51.2	42 (76.8)	8.2
W-6(a,b)	36-41.6	121-51.2	42 (76.8)	8.2
W-7(a,b)	36-38.0	121-54.0	38 (69.5)	8.6
S-1(a,b,c)	36-41.3	121.54.2	45 (82.2)	8.6
S-2(a,b,c)	36-38.3	121-56.1	52 (95.1)	8.2
S-3	36-38.3	121-56.1	52 (95.1)	8.2
S-4	36-45.1	121-55.8	57 (104.2)	8.0
S-5(a,b)	36-45.3	121-54.1	65 (118.9)	8.0
S-6(a,b)	36-48.3	121-55.0	85 (155.4)	8.5

Table I. Station Location, Water Depth and Bottom Water Temperature

Sample	Density (g/cm^3)	Penetration Depth (cm)	Frequency (H_z)	Measured Mechanical Resistance (10^4 g-cm^2/sec)
W-1a	1.65	4.49	871	3.3
			2116	7.9
			3304	17.0
W-2a	1.57	4.49	872	1.5
			2114	5.3
			3295	11.0
W-3a	1.70	4.49	874	1.9
			2115	5.5
			3308	10.0
W-4a	1.52	4.49	872	1.7
			2117	4.2
			3304	8.3
W-4b	1.52	4.49	873	1.2
			2118	4.4
			3303	8.6
W-4c	1.52	6.99	873	8.8
			2116	10.2
			3302	20.0
W-5a	1.50	4.49	874	2.9
			2115	5.1
			3306	9.1
W-5b	1.50	6.0	872	2.0
			2112	7.2
			3301	14.0
W-6a	1.51	4.49	875	0.88
			2114	3.8
			3306	6.8
W-6b	1.51	4.49	872	1.4
			2114	5.0
			3303	9.2
W-7a	1.57	4.49	872	1.8
			2114	4.5
			3299	8.4
W-7b	1.57	4.49	876	4.3
			2114	9.0

Table II. Measured Torsional Impedance of Sediments

Sample	Density (g/cm^3)	Penetration Depth (cm)	Frequency (Hz)	Measured Mechanical Resistance (10^4 g-cm^2/sec)
S-1a	1.48	4.79	875	9.0
			2111	12.0
			3306	23.0
S-1b	1.48	6.79	880	14.0
			2112	17.0
			3309	27.0
S-1c	1.48	7.49	874	9.4
			2115	11.0
			3269	20.0
S-2a	1.45	4.49	876	4.3
			2119	6.4
			3303	13.0
S-2b	1.45	6.99	881	15.0
			2121	17.0
			3313	26.0
S-3	1.43	4.49	872	3.8
			2118	6.0
			3300	14.0
S-4	1.82	4.49	890	16.0
			2119	15.0
			3300	29.0
S-5a	1.86	4.49	920	32.0
			2134	21.0
			3344	27.0
S-5b	1.86	5.0	939	37.0
			2133	26.0
			3350	29.0
S-6a	1.95	4.49	874	11.0
			2118	12.0
			3293	25.0
S-6b	1.95	4.89	872	4.9
			2113	8.1
			3292	20.0

Table II. Measured Torsional Impedance of Sediments (Cont.)

Sample	Density (g/cm^3)	Penetration Depth (cm)	Frequency (Hz)	Measured Mechanical Resistance (10^4 g-cm^2/sec)
W-1b	1.65	4.49	882	13.0
			2117	16.0
			3313	26.0
W-2b	1.57	4.49	879	13.0
			2120	14.0
			3318	22.0
W-3b	1.48	6.0	887	16.0
			2121	20.0
			3321	28.0

*Measurements were taken in an elevated and drained region of the sample.

Table III. Measured Torsional Impedance of Sediments Under Dry* Conditions.

Sample	Density (g/cm^3)	Penetration Depth (cm)	Frequency (Hz)	Measured Mechanical Resistance (10^4 g-cm^2/sec)
W-1	1.63	4.49	891	0.49
			2138	2.8
			3375	1.2
W-2	1.57	4.49	892	1.6
			2138	3.3
			3375	1.6
W-3	1.48	4.49	891	—
			2139	2.1
			3376	—
W-4	1.52	4.49	892	1.1
			2137	2.6
			3375	1.2
W-5	1.50	4.49	892	1.4
			2137	3.3
			3375	1.6
W-6	1.51	4.49	892	2.3
			2139	3.2
			3375	1.4
W-7	1.57	4.49	892	2.9
			2139	4.1
			3376	2.3

*Measurements taken after sediments were mixed thoroughly.

Table IV. Measured Torsional Impedance of Sediments Under Mixed* Conditions

Sample	Wet Density (g/cm^3)	Porosity (%)	Vane Shear Strength (psi)
W-1a	1.63	66.9	0.046
W-1b	1.63	66.9	——
W-2a	1.57	70.6	0.071
W-2b	1.57	70.6	0.573
W-3a	1.48	73.0	0.081
W-3b	1.48	73.0	0.396
W-4a	1.52	72.0	0.085
W-4b	1.52	72.0	0.363
W-4c	1.52	72.0	——
W-5a	1.50	70.7	——
W-5b	1.50	70.7	0.152
W-6a	1.51	76.5	0.085
W-6b	1.51	76.5	0.085
W-7a	1.57	73.0	0.195
W-7b	1.57	73.0	0.195
S-1a	1.48	69.9	0.120
S-1b	1.48	69.9	——
S-1c	1.48	69.9	——
S-2a	1.45	73.1	0.099
S-2b	1.45	73.1	——
S-3	1.43	72.5	0.079
S-4	1.82	52.9	0.185
S-5a	1.86	49.4	0.297
S-5b	1.86	49.4	——
S-6a	1.95	57.3	0.292
S-6b	1.95	57.3	0.292

Table V. Mass Physical Properties of Sediments

Sample	*Csed/ Cwater	Compressional Wave Speed (m/sec)	ρC_{sed}^2 (10^6g-m^2/cm^2-sec^2)
W-1(a,b)	1.004	1489.3	3.615
W-2(a,b)	1.010	1499.0	3.438
W-3(a,b)	1.014	1504.9	3.352
W-4(a,b,c)	1.011	1500.4	3.422
W-5(a,b)	1.017	1508.9	3.415
W-6(a,b)	1.010	1498.5	3.391
W-7(a,b)	1.006	1494.1	3.505
S-1(a,b,c)	1.009	1499.4	3.327
S-2(a,b)	1.012	1501.1	3.267
S-3	1.008	1496.0	3.200
S-4	0.922	1367.1	3.402
S-5(a,b)	0.927	1375.4	3.519
S-6(a,b)	0.970	1441.9	4.054

*Laboratory sediment-to-water sound speed ratio.

Table VI. Acoustic Properties of Sediments

Sample	Mean Grain Size (Ø)	Sorting (Deviation)	Sand (%)	Silt (%)	Clay (%)	Gravel (%)
W-1(a,b)	5.27	1.79	31.18	64.23	4.59	0.00
W-2(a,b)	5.31	1.81	29.58	68.92	1.08	0.42
W-3(a,b)	6.73	1.29	1.62	85.99	12.39	0.00
W-4(a,b,c)	6.72	1.28	0.0	82.84	17.16	0.29
W-5(a,b)	6.50	0.49	1.25	81.69	17.05	0.00
W-6(a,b)	6.53	1.36	1.07	82.32	16.61	0.00
W-7(a,b)	5.78	1.10	2.79	90.18	7.04	0.00
S-1(a,b,c)	6.46	1.01	1.05	91.00	7.95	0.00
5-2(a,b)	6.43	0.91	1.15	92.10	6.75	0.00
5-3	6.32	0.98	1.57	91.12	7.31	0.00
5-4	1.40	4.01	51.18	14.03	5.94	28.84
5-5(a,b)	1.69	2.52	74.14	10.33	1.34	14.20
5-6(a,b)	4.55	2.48	50.92	35.15	12.68	1.25

Table VII. Textural Analysis of Sediments

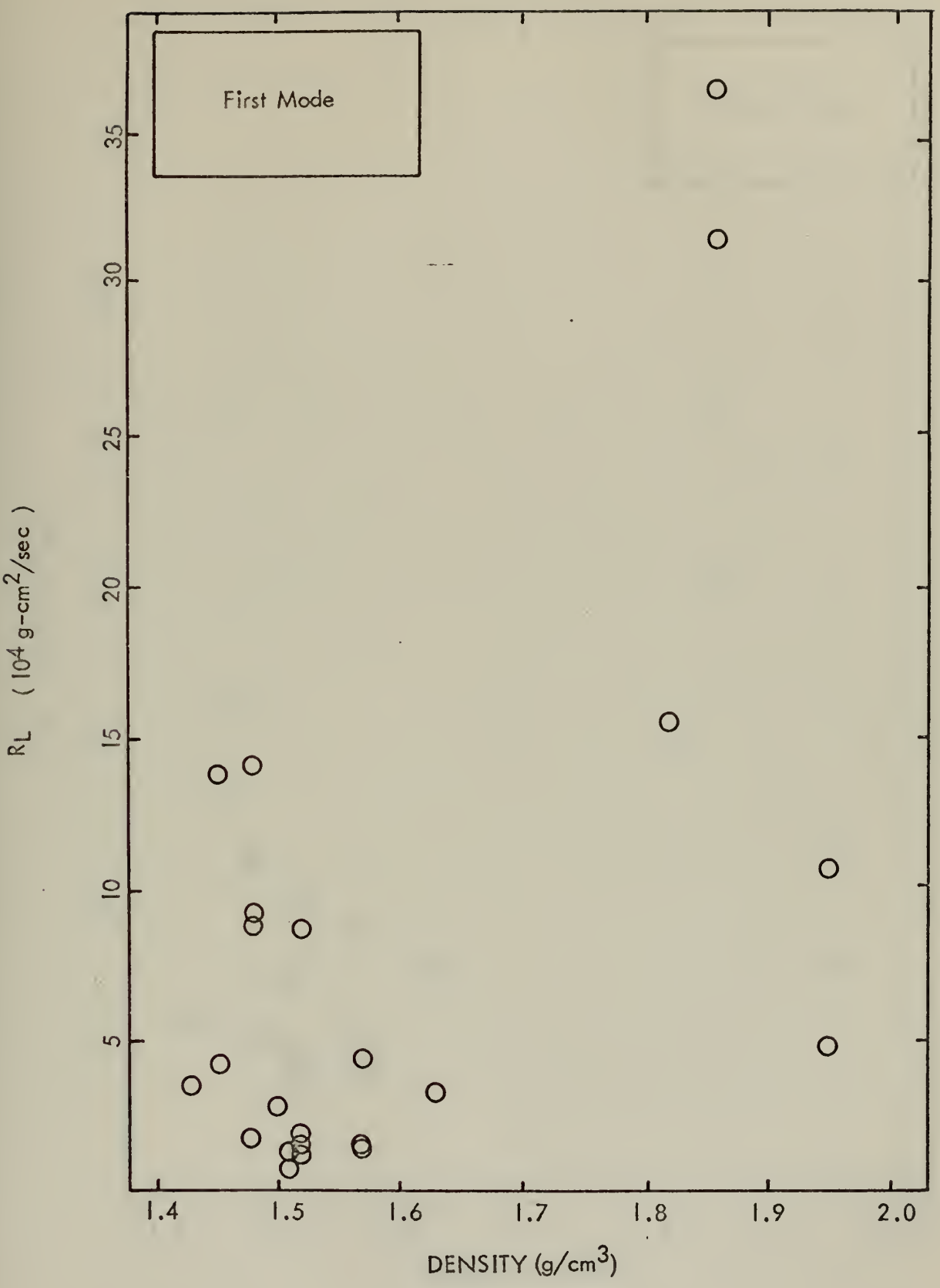

Figure 7. R_L as a Function of Wet Density, First Mode

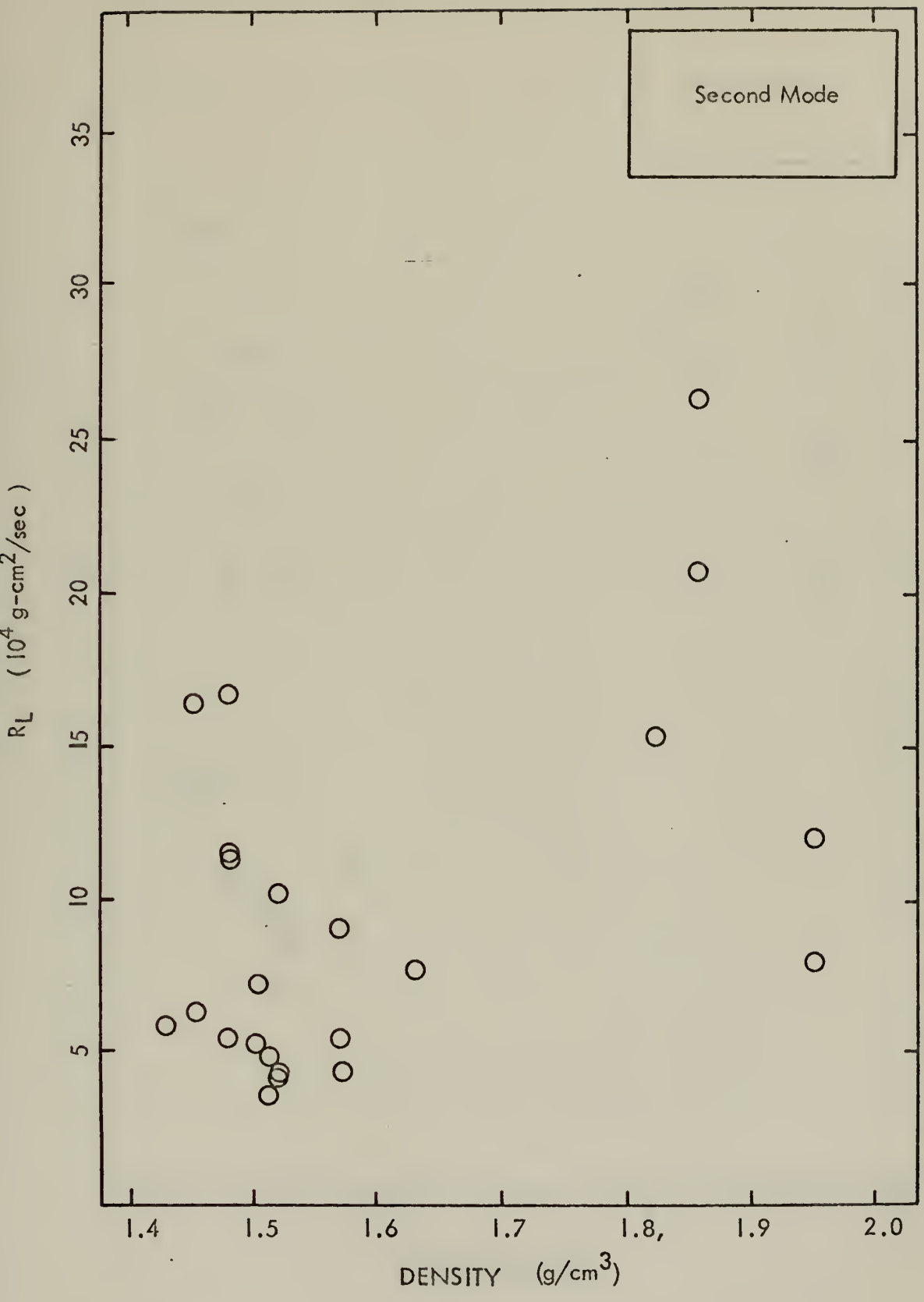

Figure 8. R_L as a Function of Wet Density, Second Mode

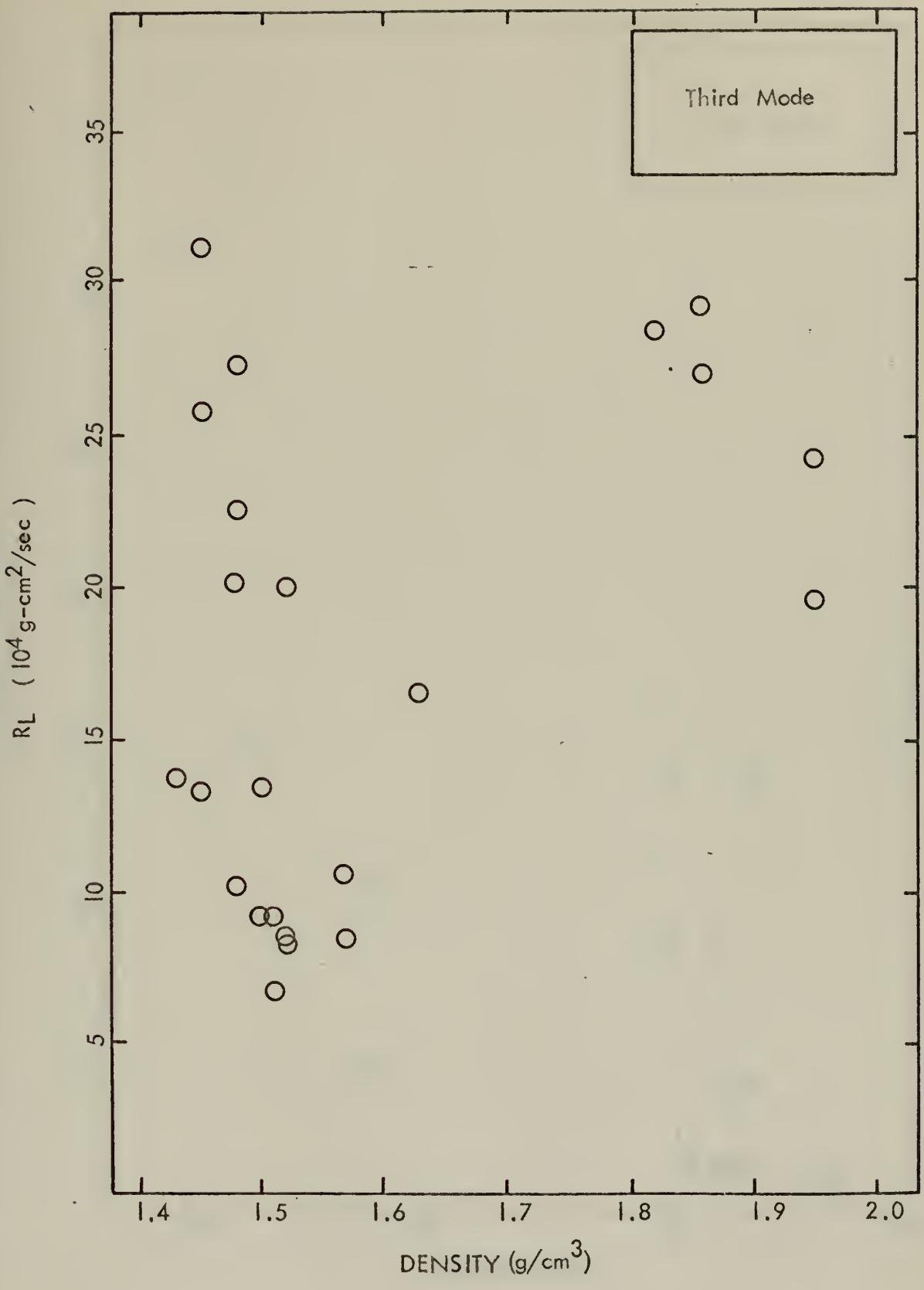

Figure 9. R_L as a Function of Wet Density, Third Mode

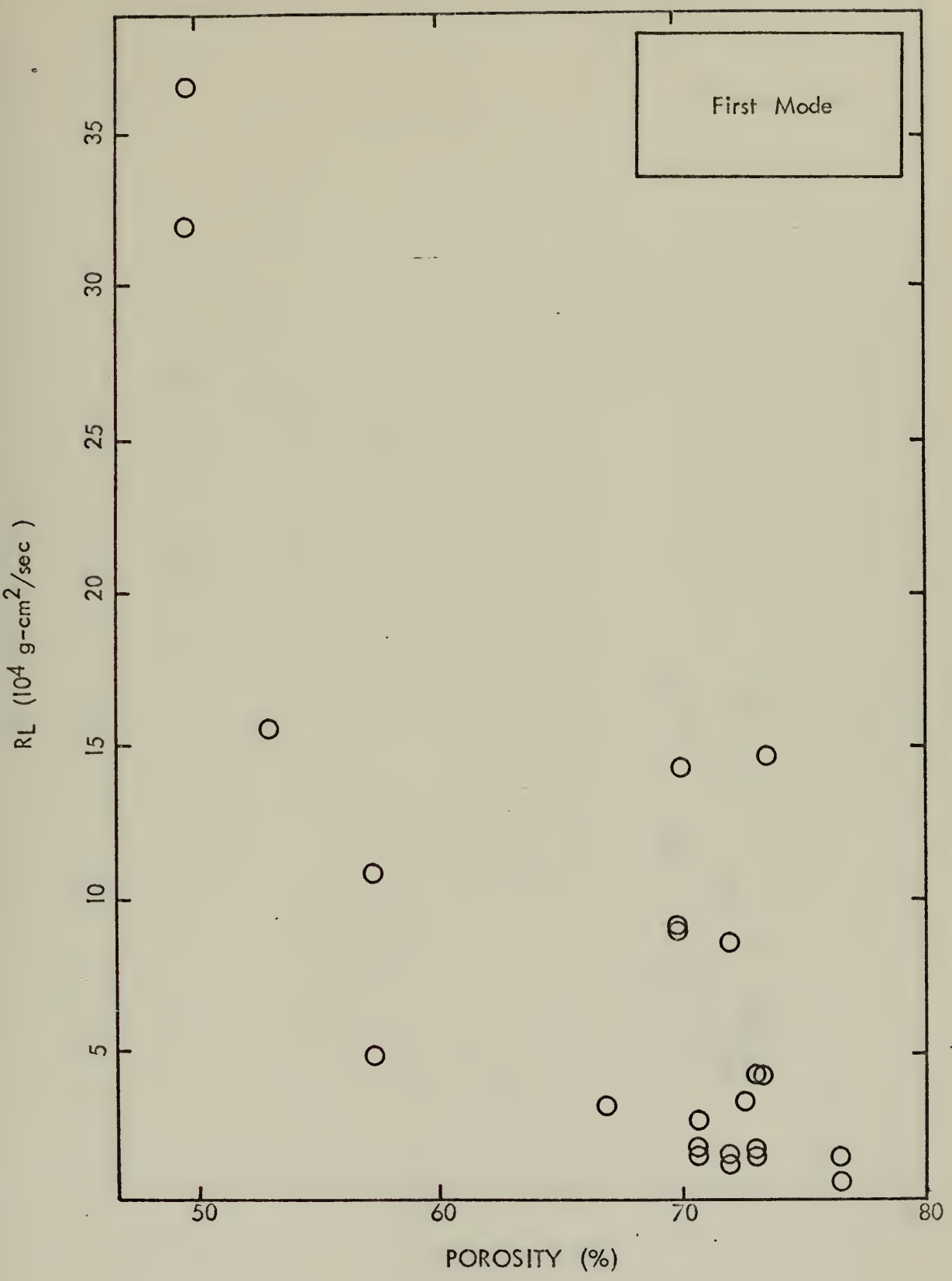

Figure 10. R_L as a Function of Porosity, First Mode

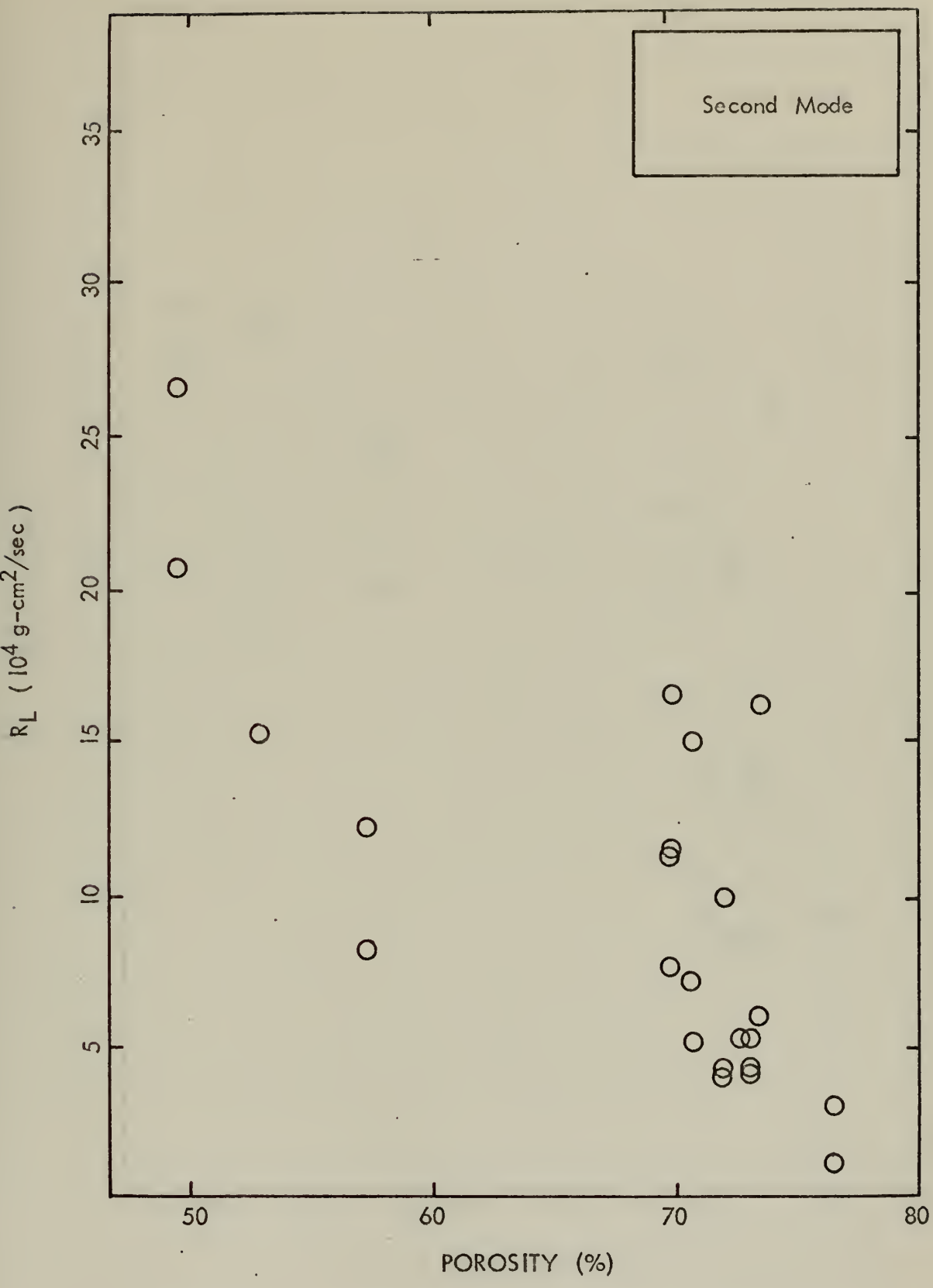

Figure 11. R_L as a Function of Porosity, Second Mode

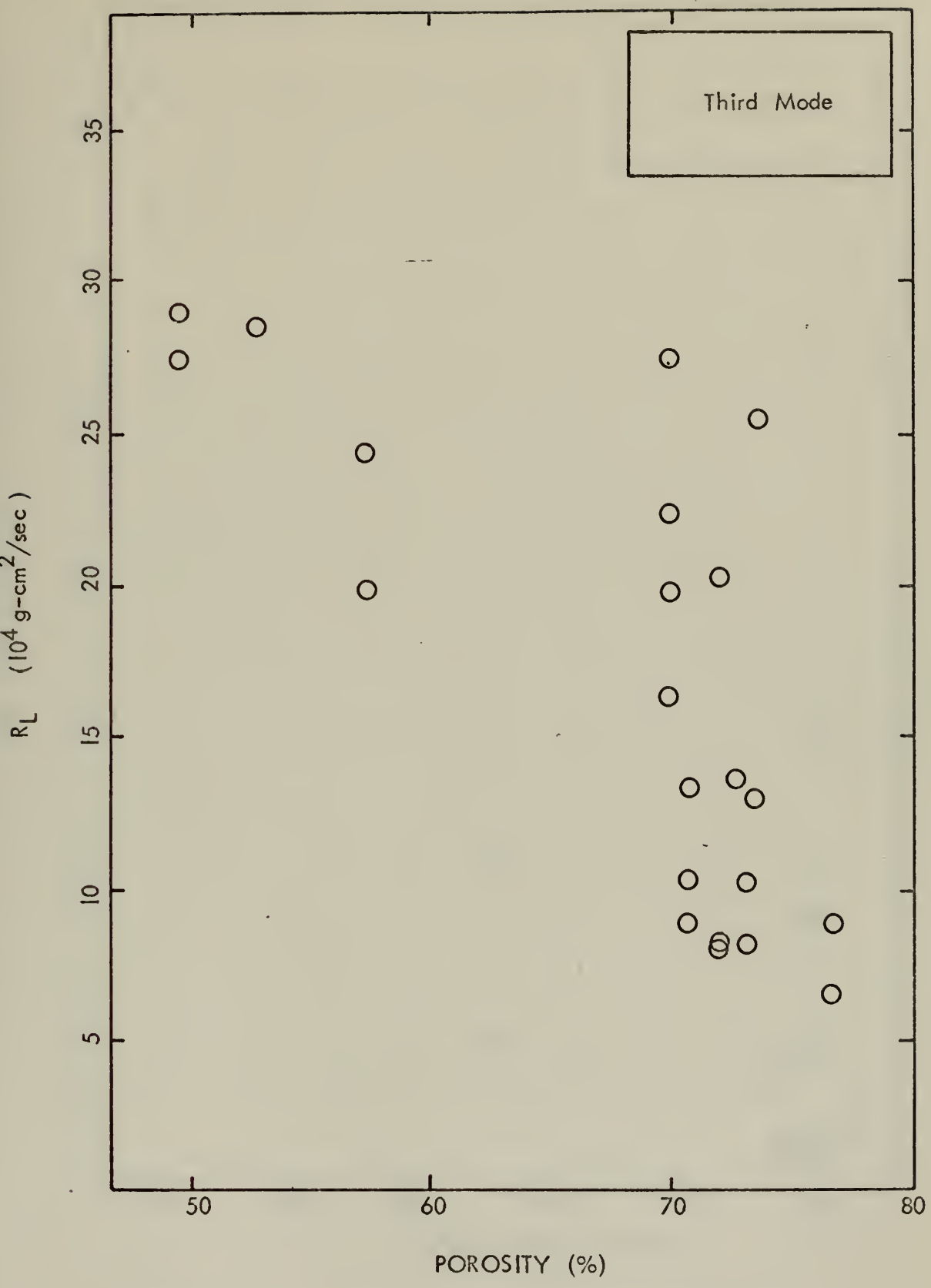

Figure 12. R_L as a Function of Porosity, Third Mode

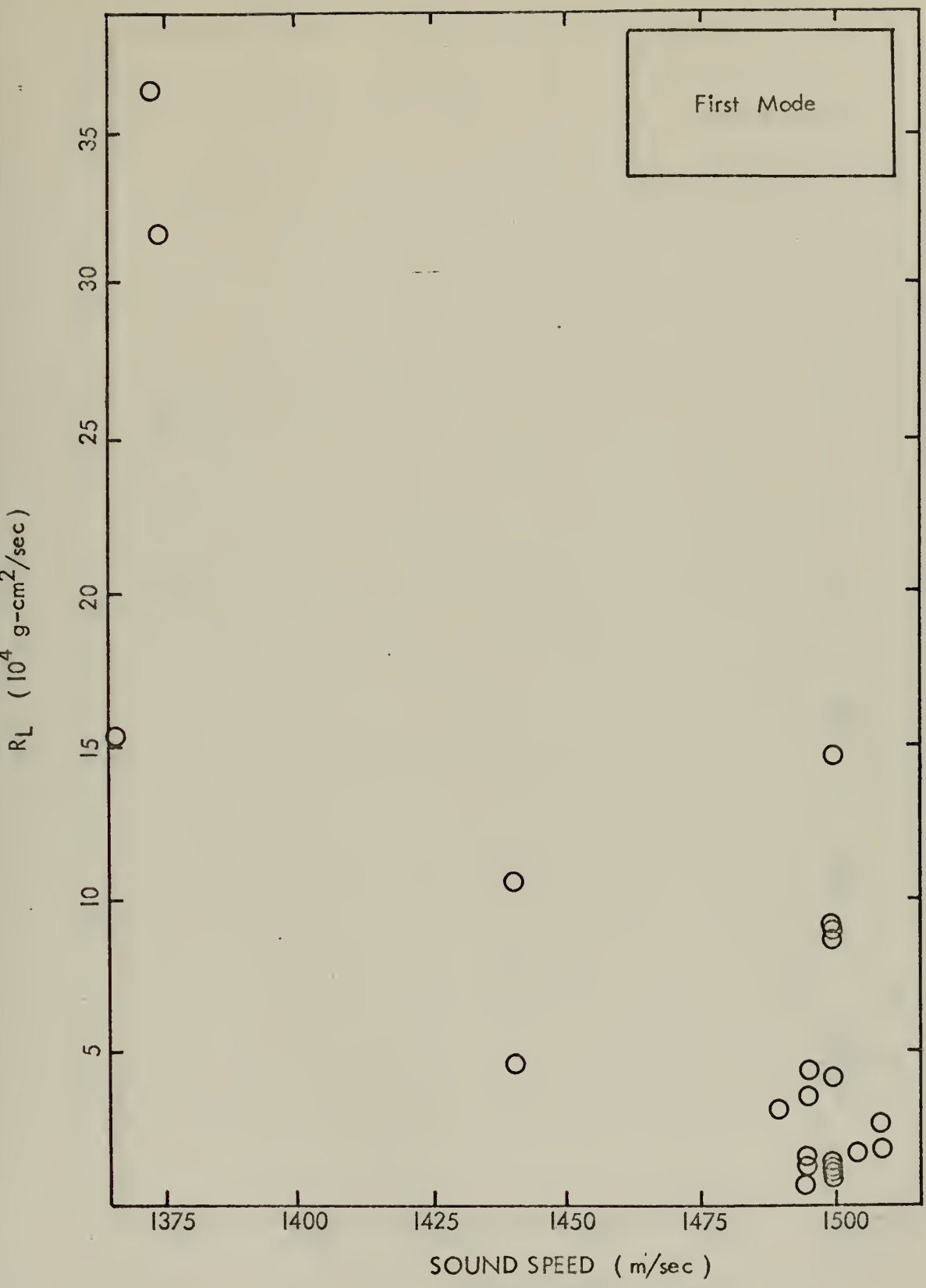

Figure 13. R_L as a Function of Sound Speed, First Mode

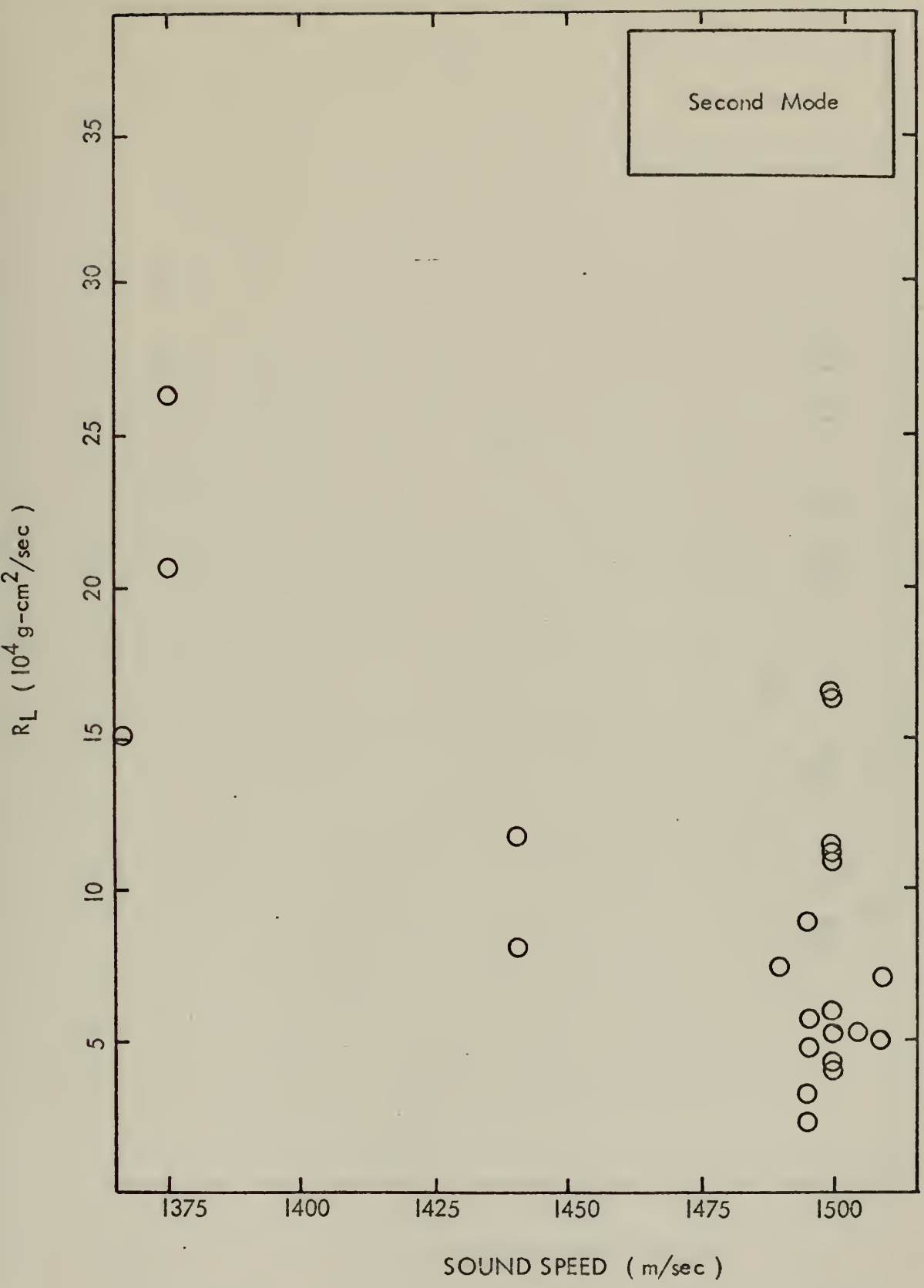

Figure 14. R_L as a Function of Sound Speed, Second Mode

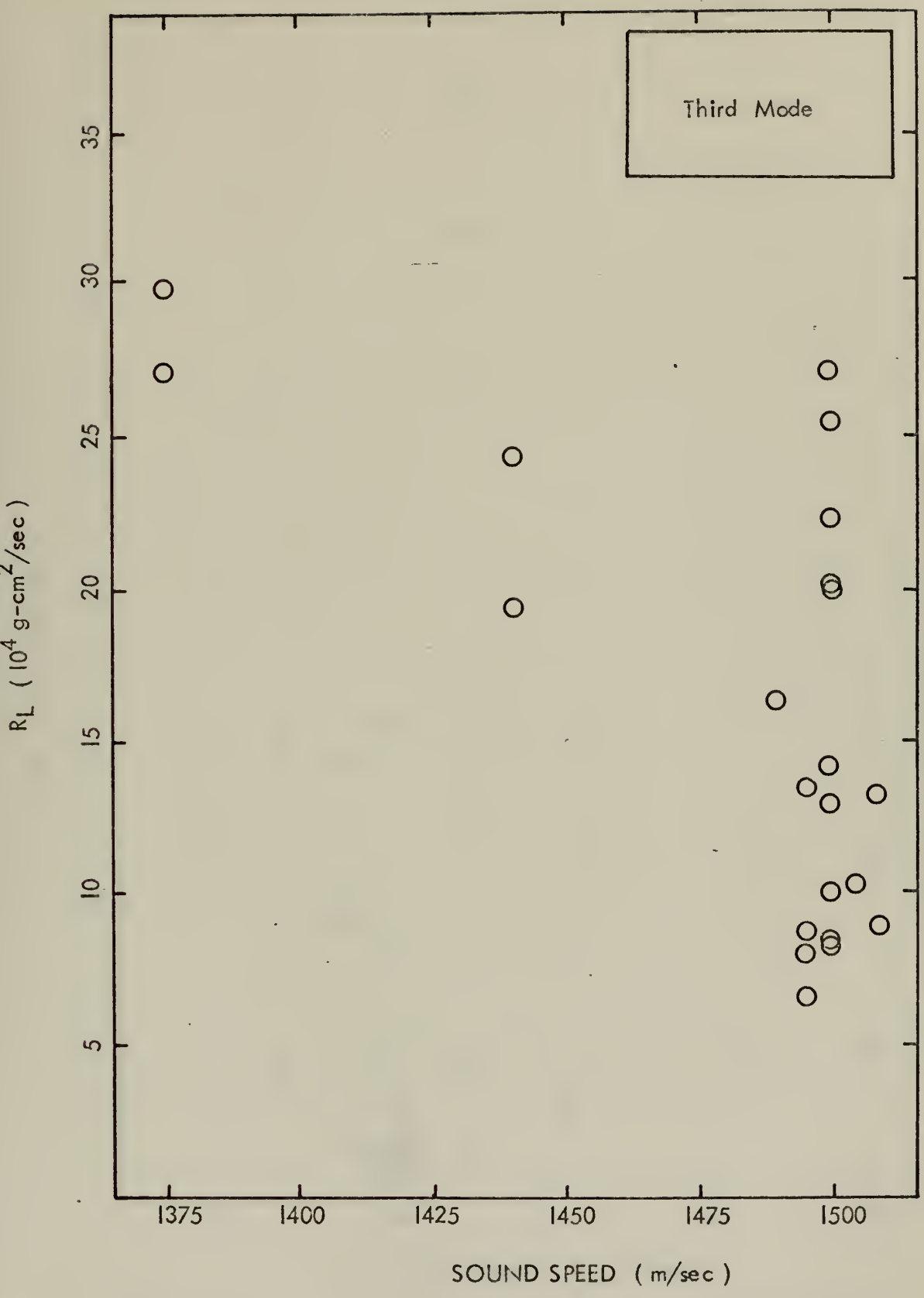

Figure 15. R_L as a Function of Sound Speed, Third Mode

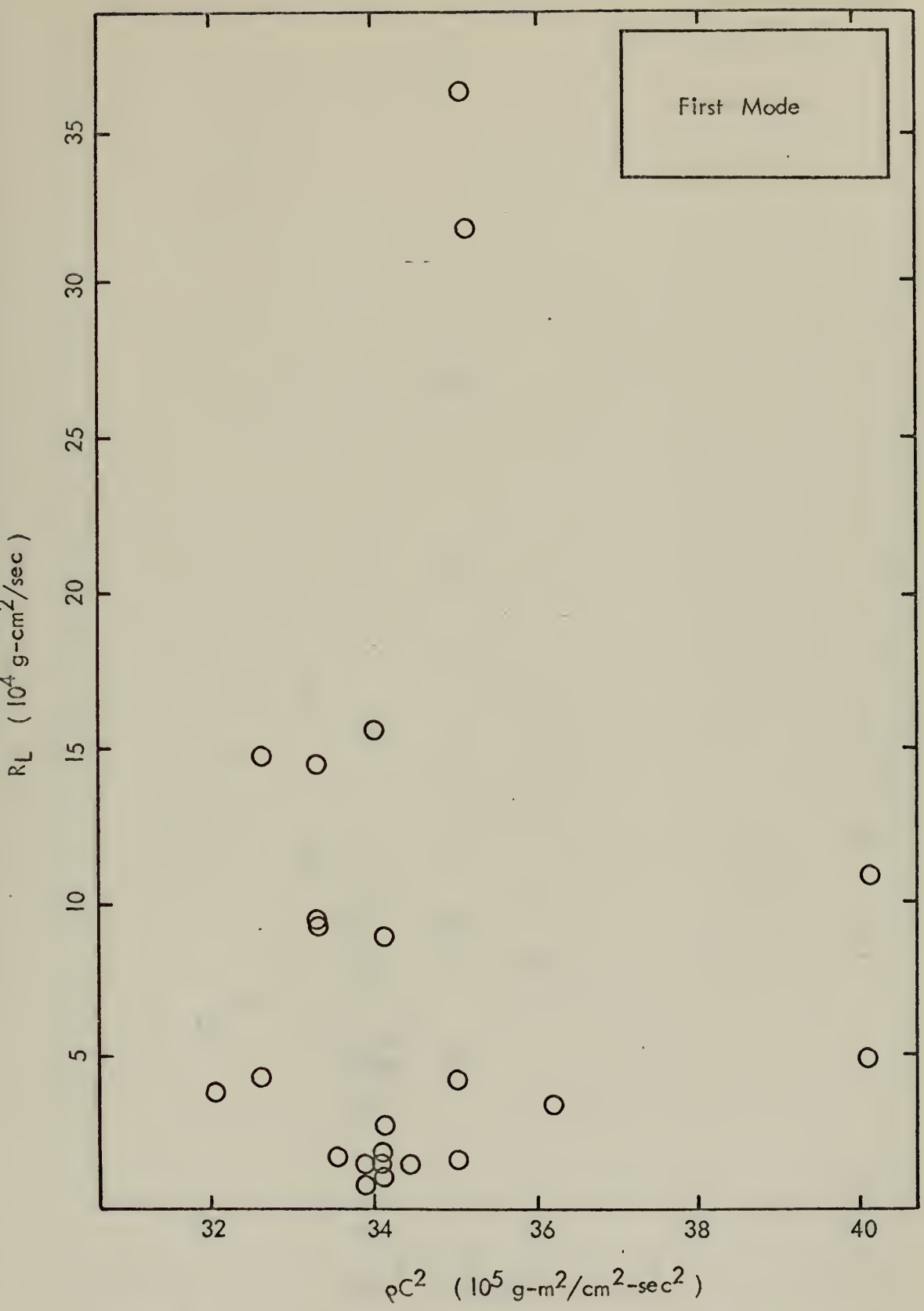

Figure 16. R_L as a Function of the Product of Wet Density and Sound Speed Squared, First Mode

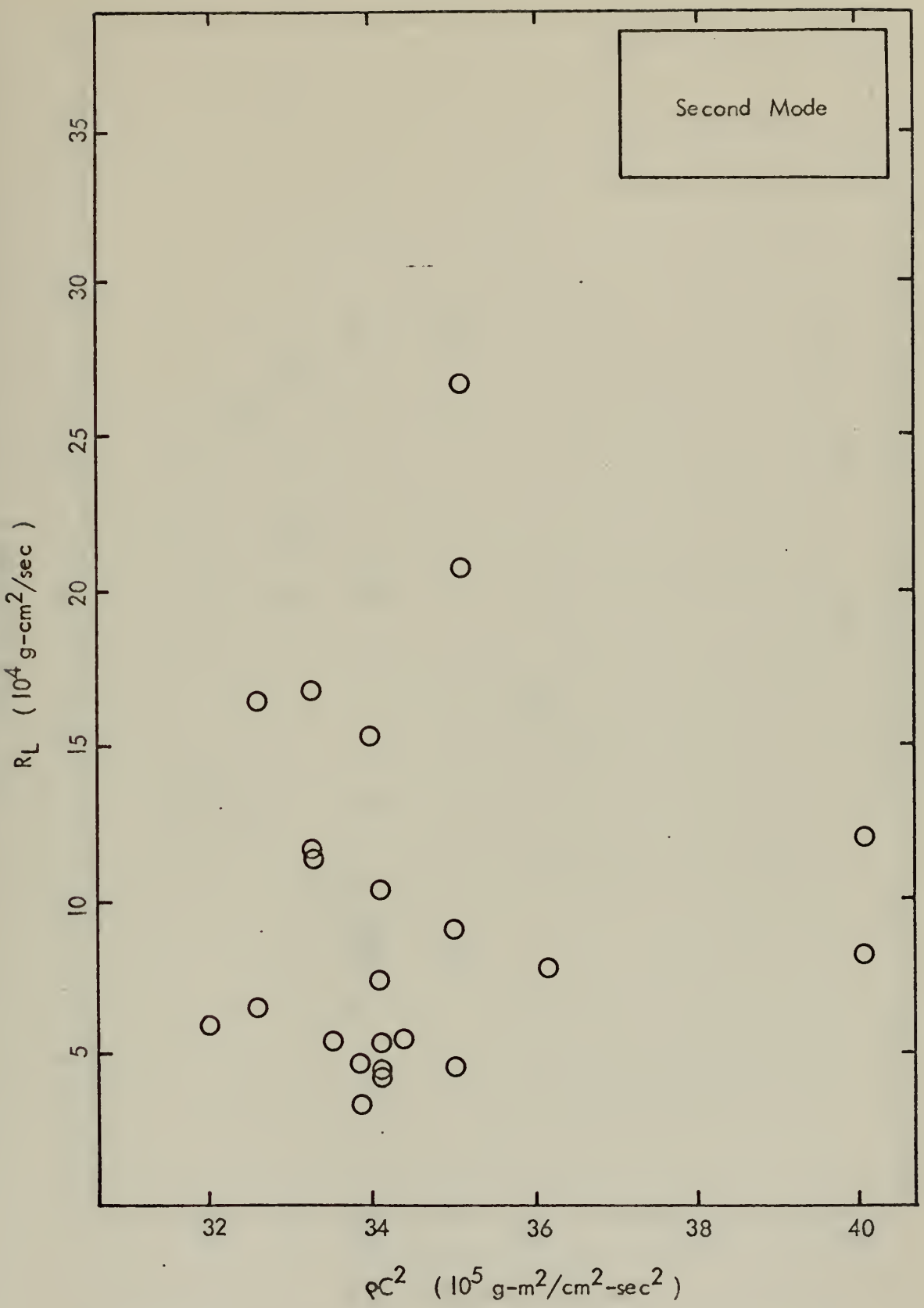

Figure 17. R_L as a Function of the Product of Wet Density and Sound Speed Squared, Second Mode

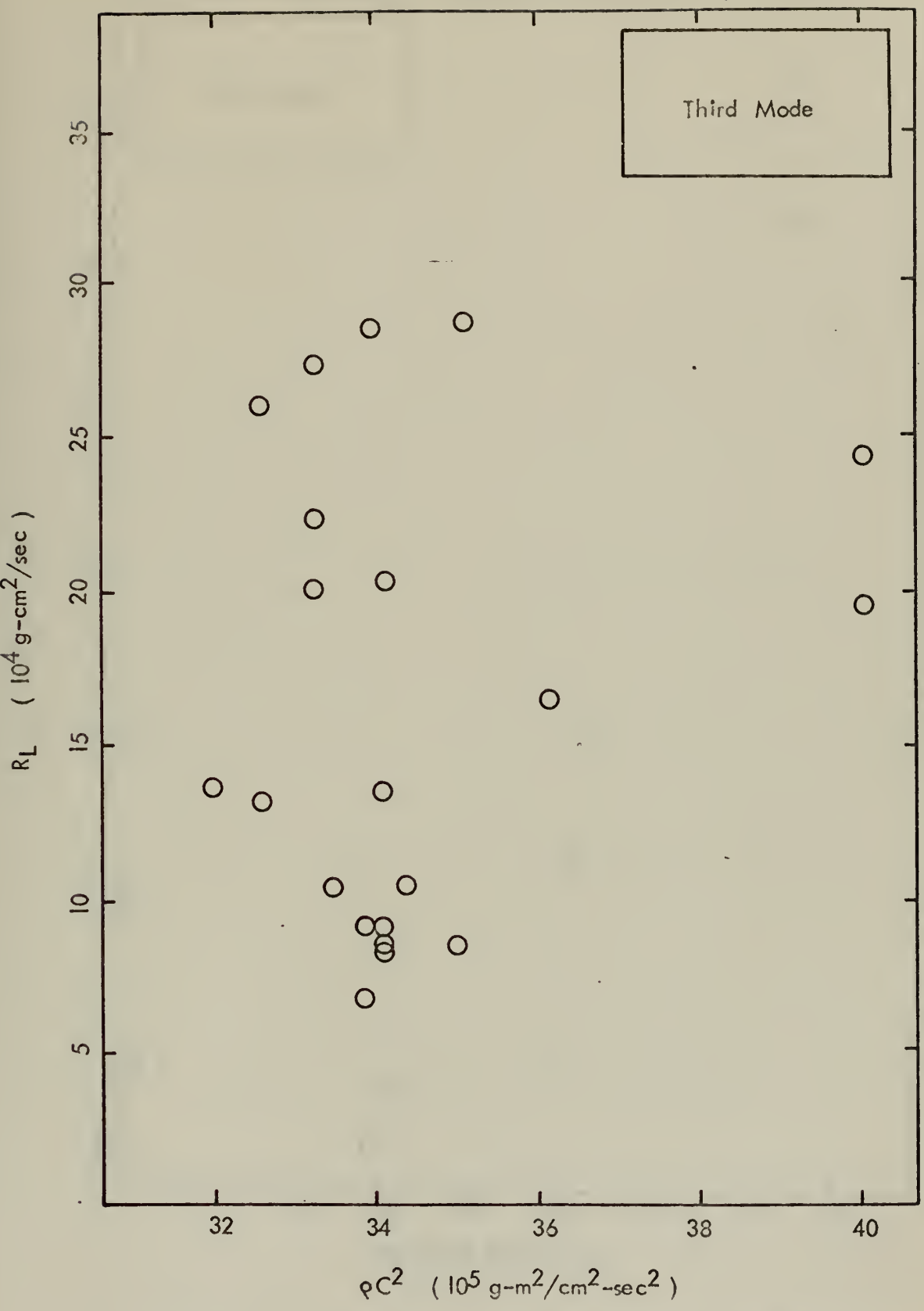

Figure 18. R_L as a Function of the Product of Wet Density and Sound Speed Squared, Third Mode

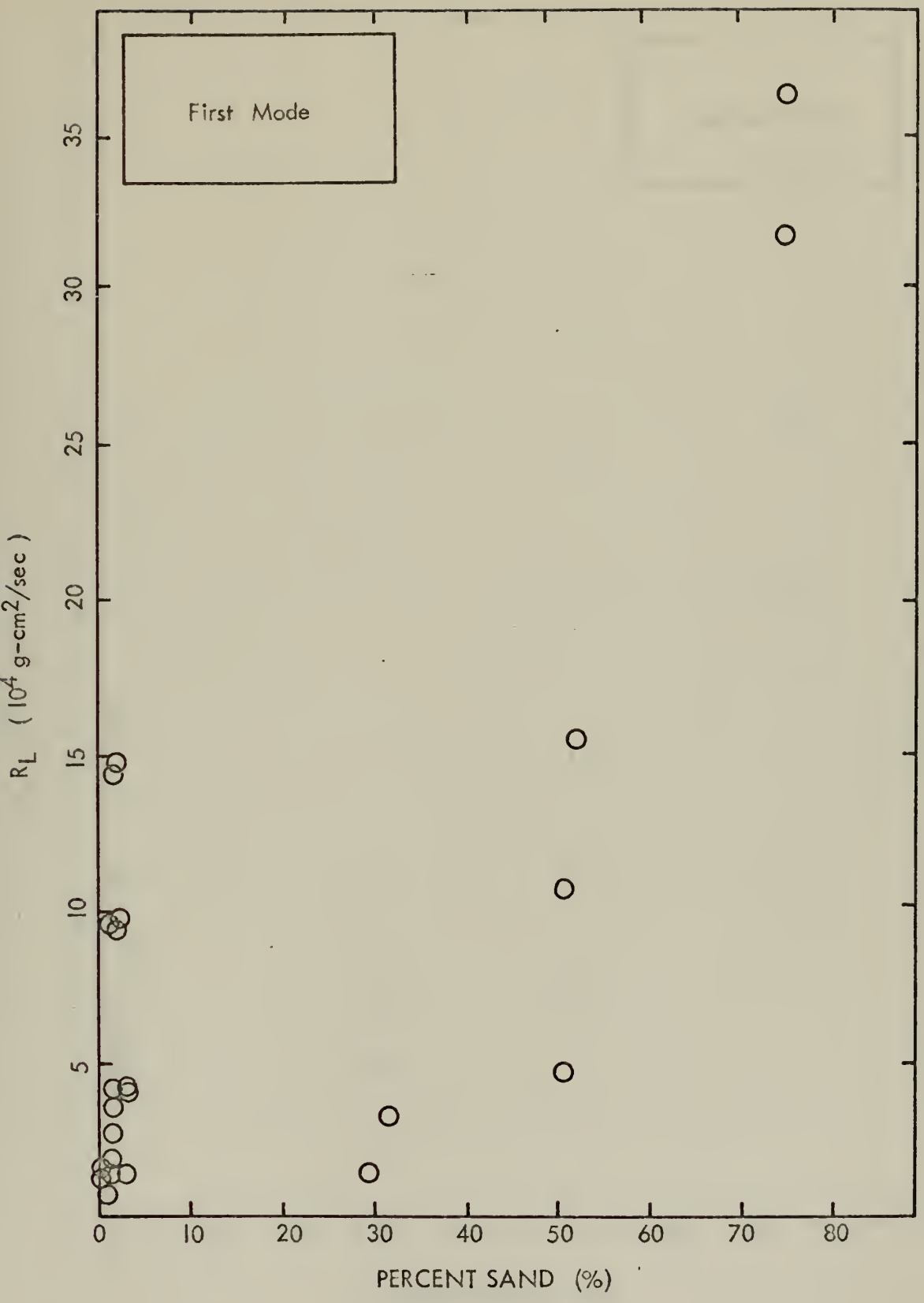

Figure 19. R_L as a Function of Percent Sand, First Mode

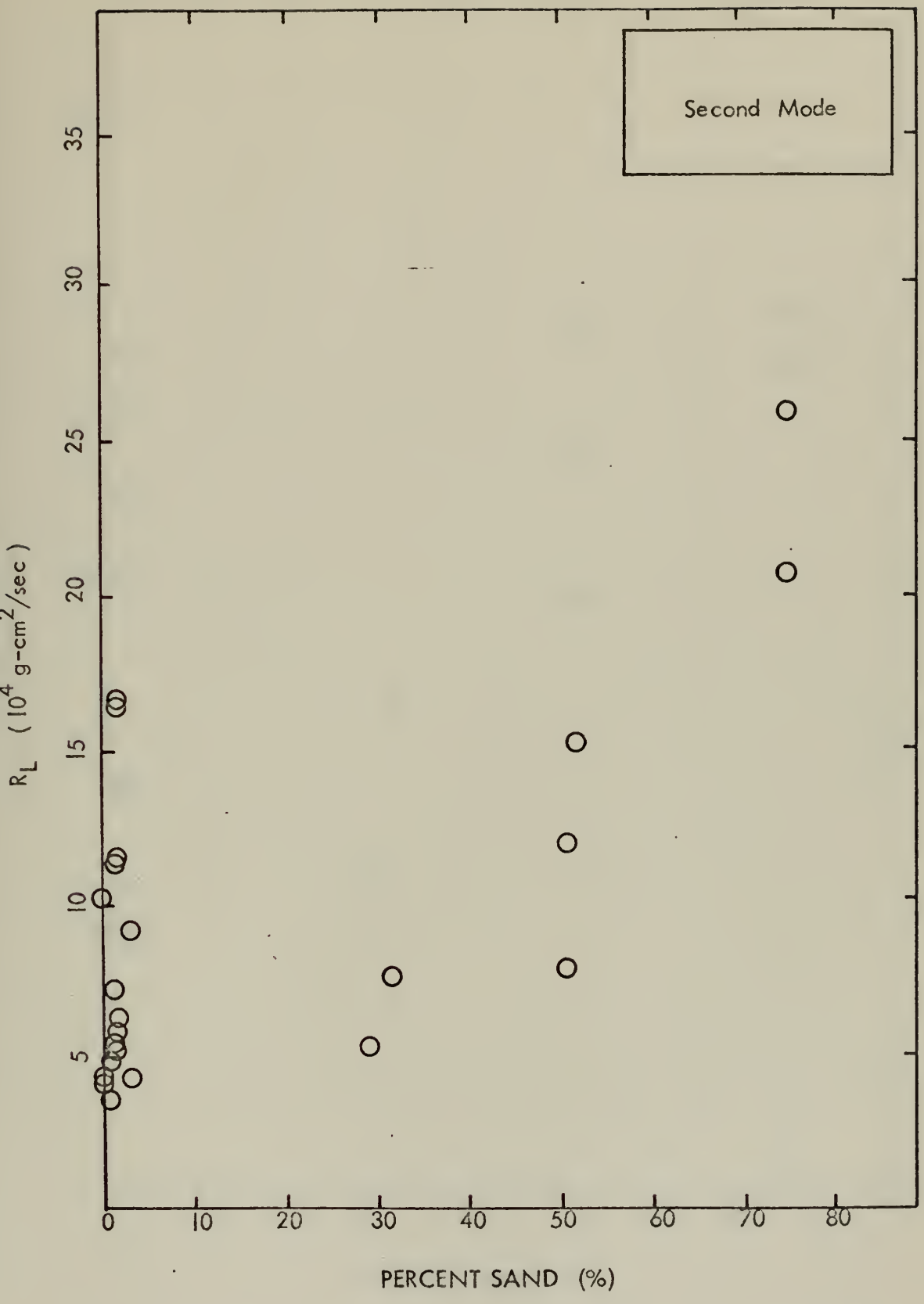

Figure 20. R_L as a Function of Percent Sand, Second Mode

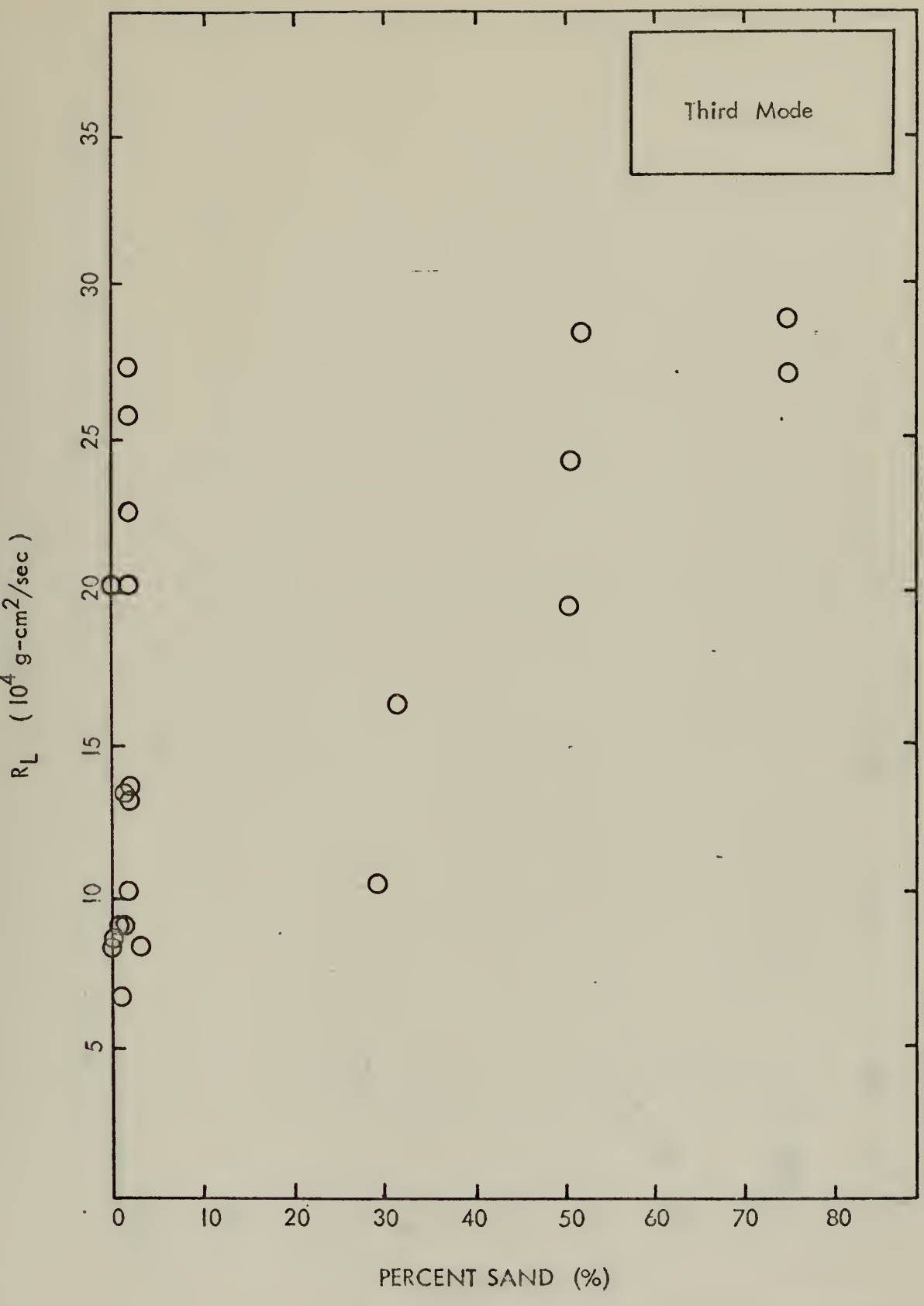

Figure 21. R_L as a Function of Percent Sand, Third Mode

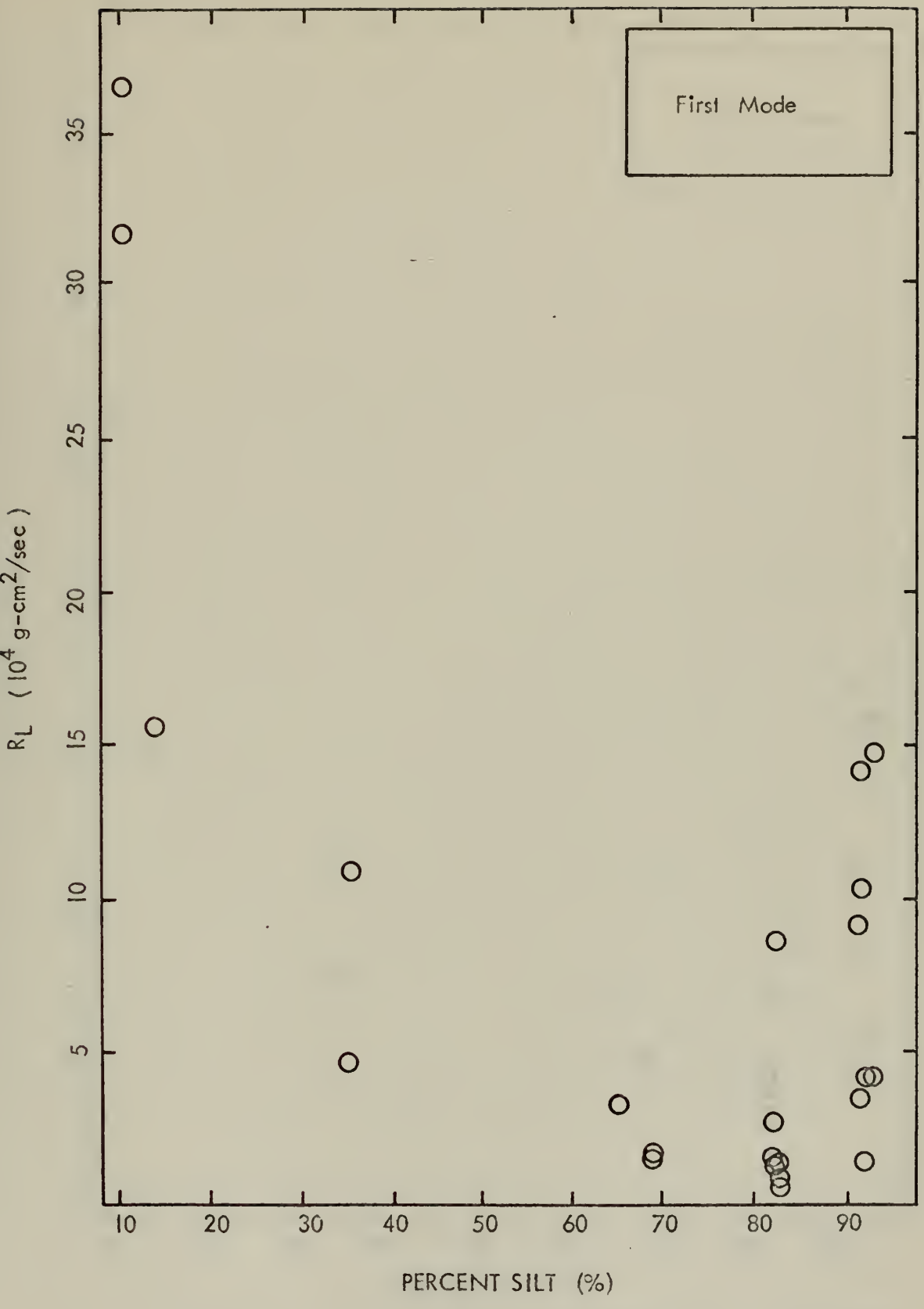

Figure 22. R_L as a Function of Percent Silt, First Mode

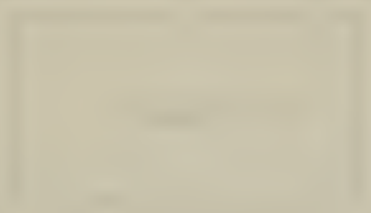

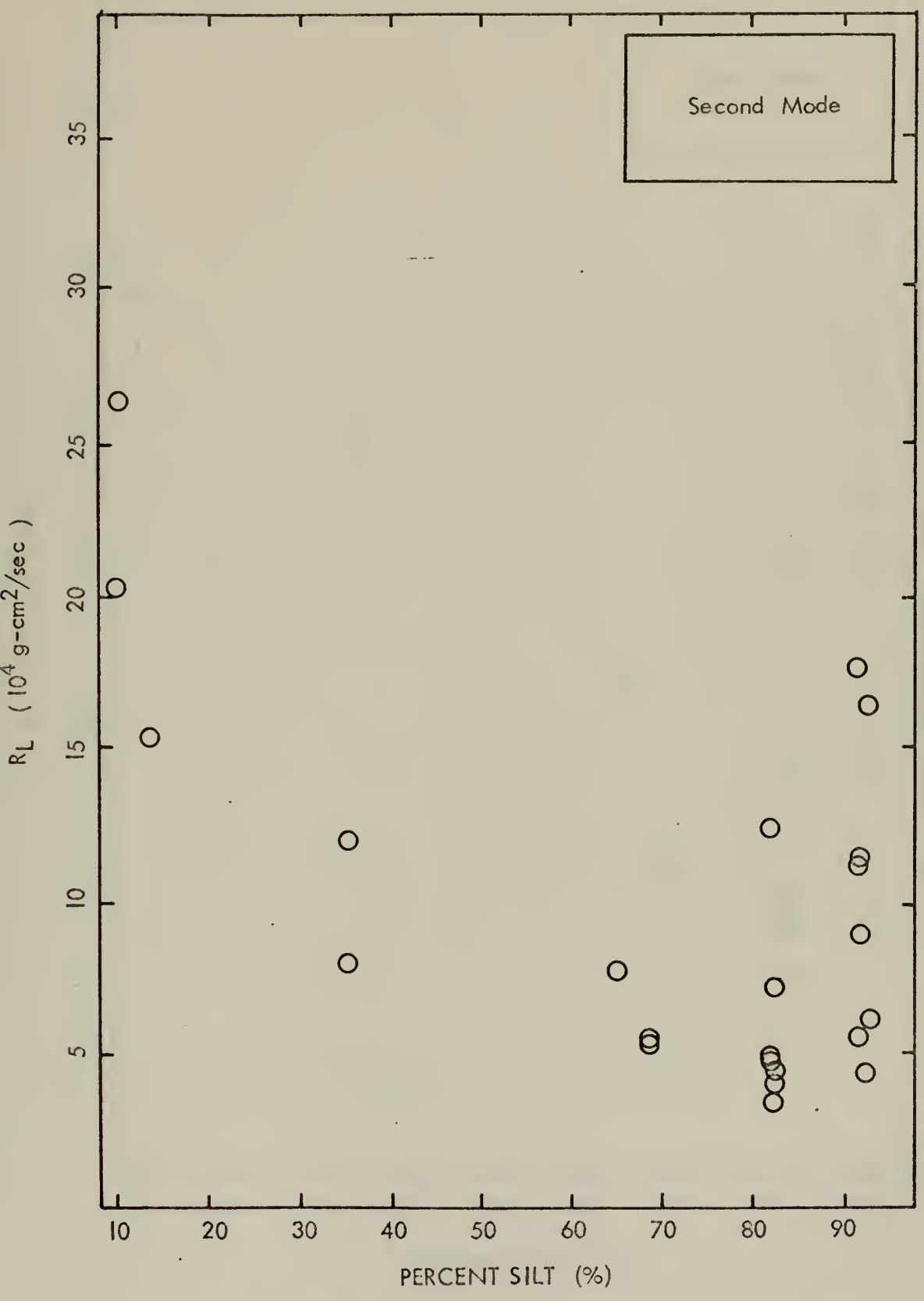

Figure 23. R_L as a Function of Percent Silt, Second Mode

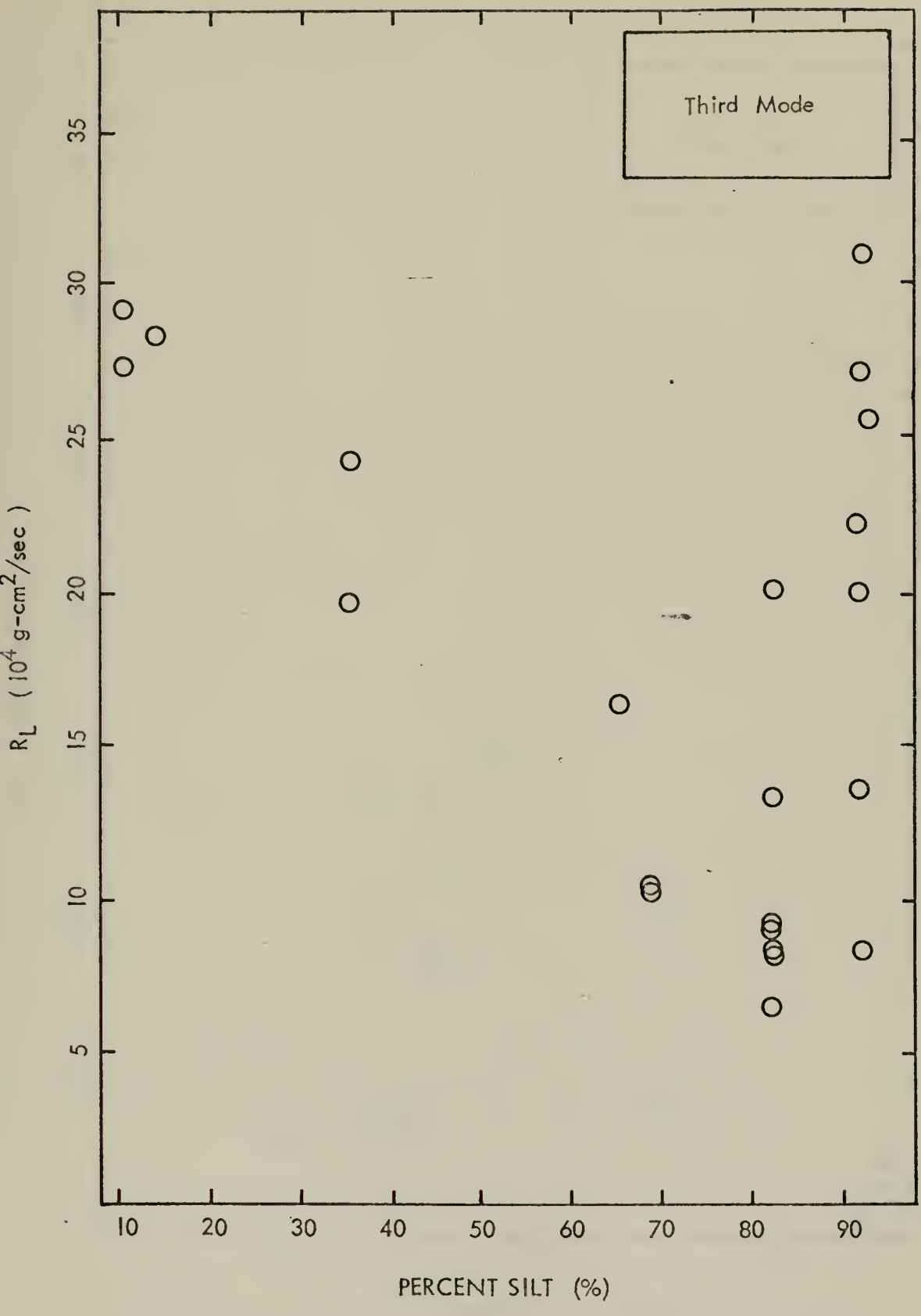

Figure 24. R_L as a Function of Percent Silt, Third Mode

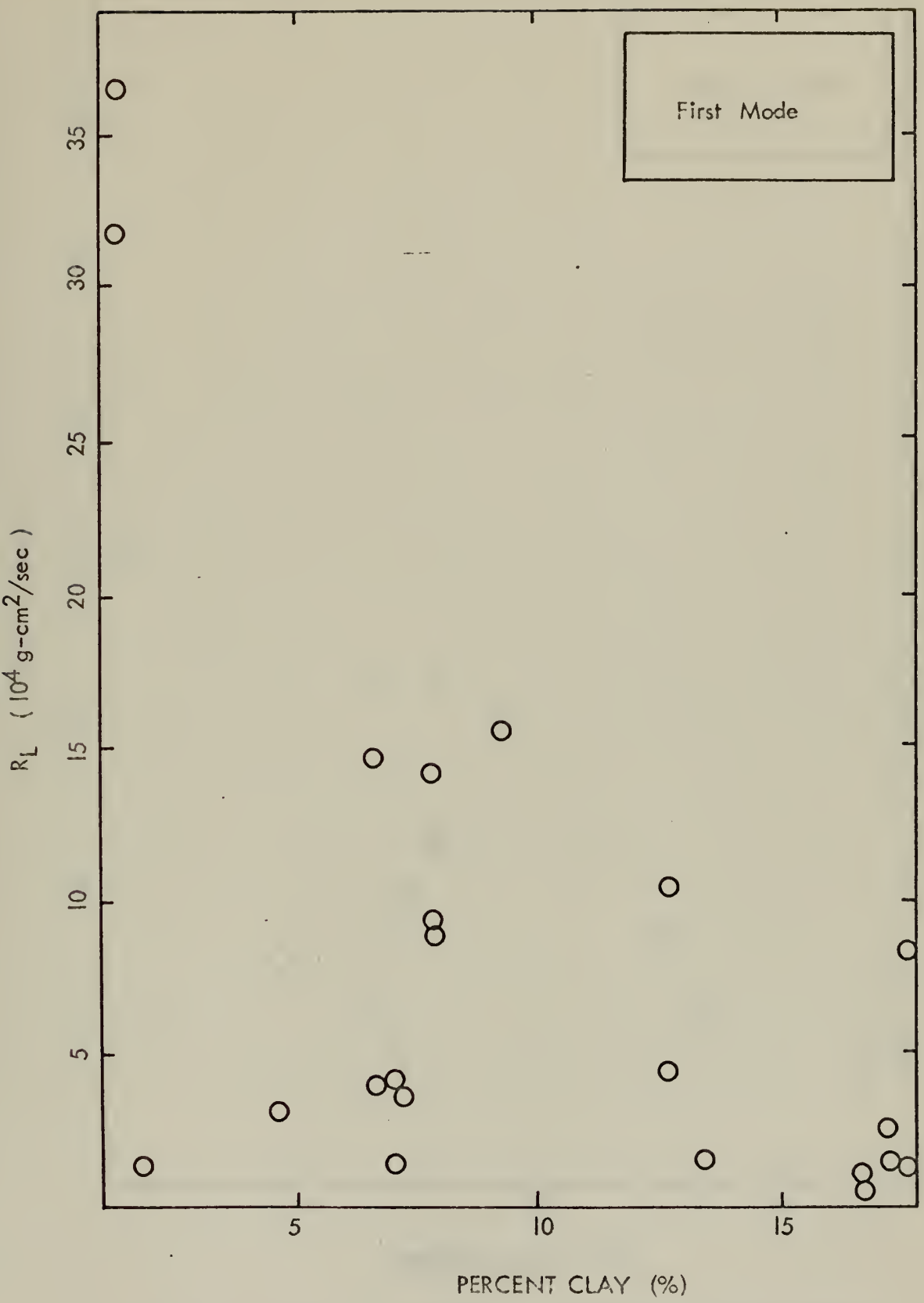

Figure 25. R_L as a Function of Percent Clay, First Mode

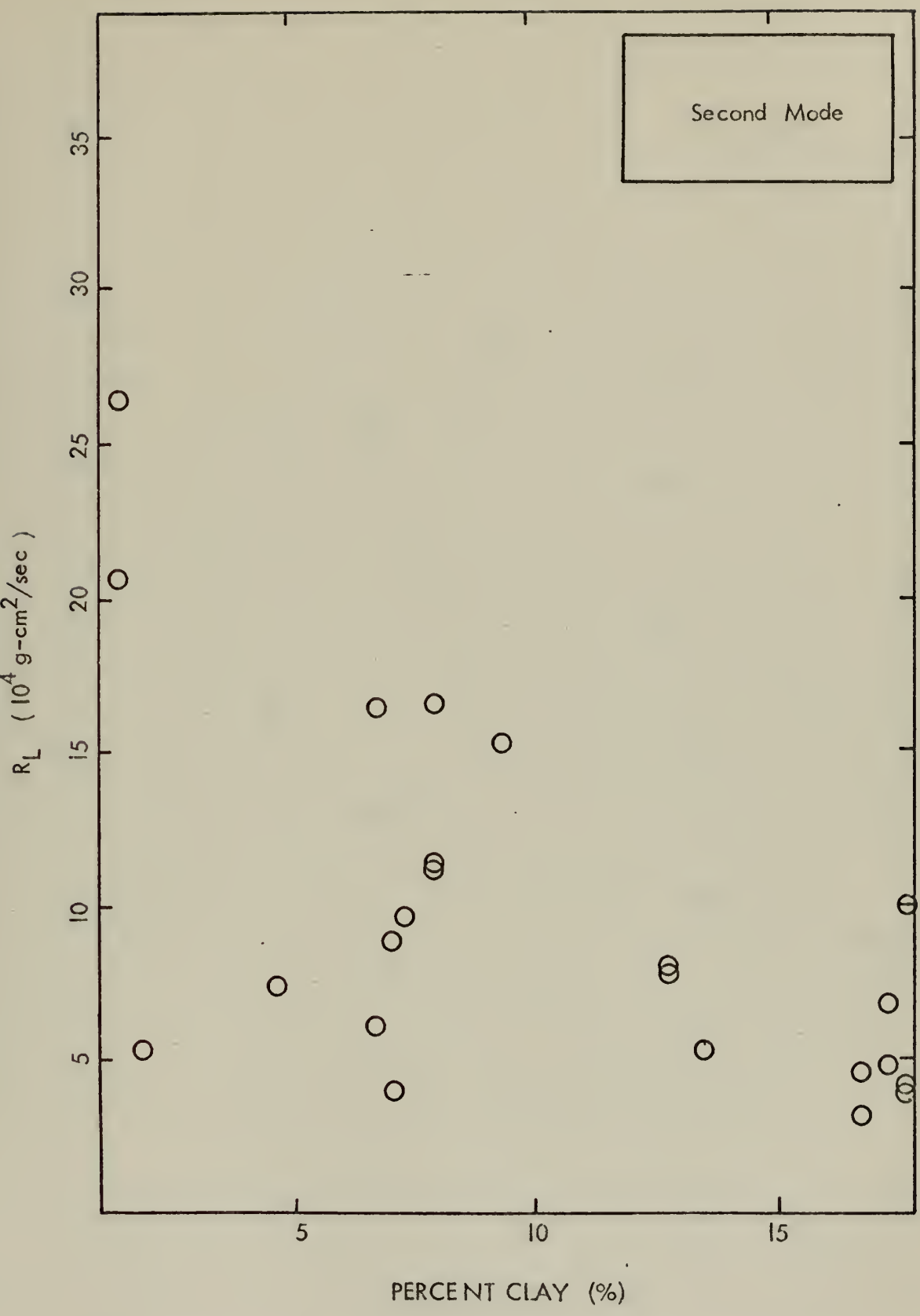

Figure 26. R_L as a Function of Percent Clay, Second Mode

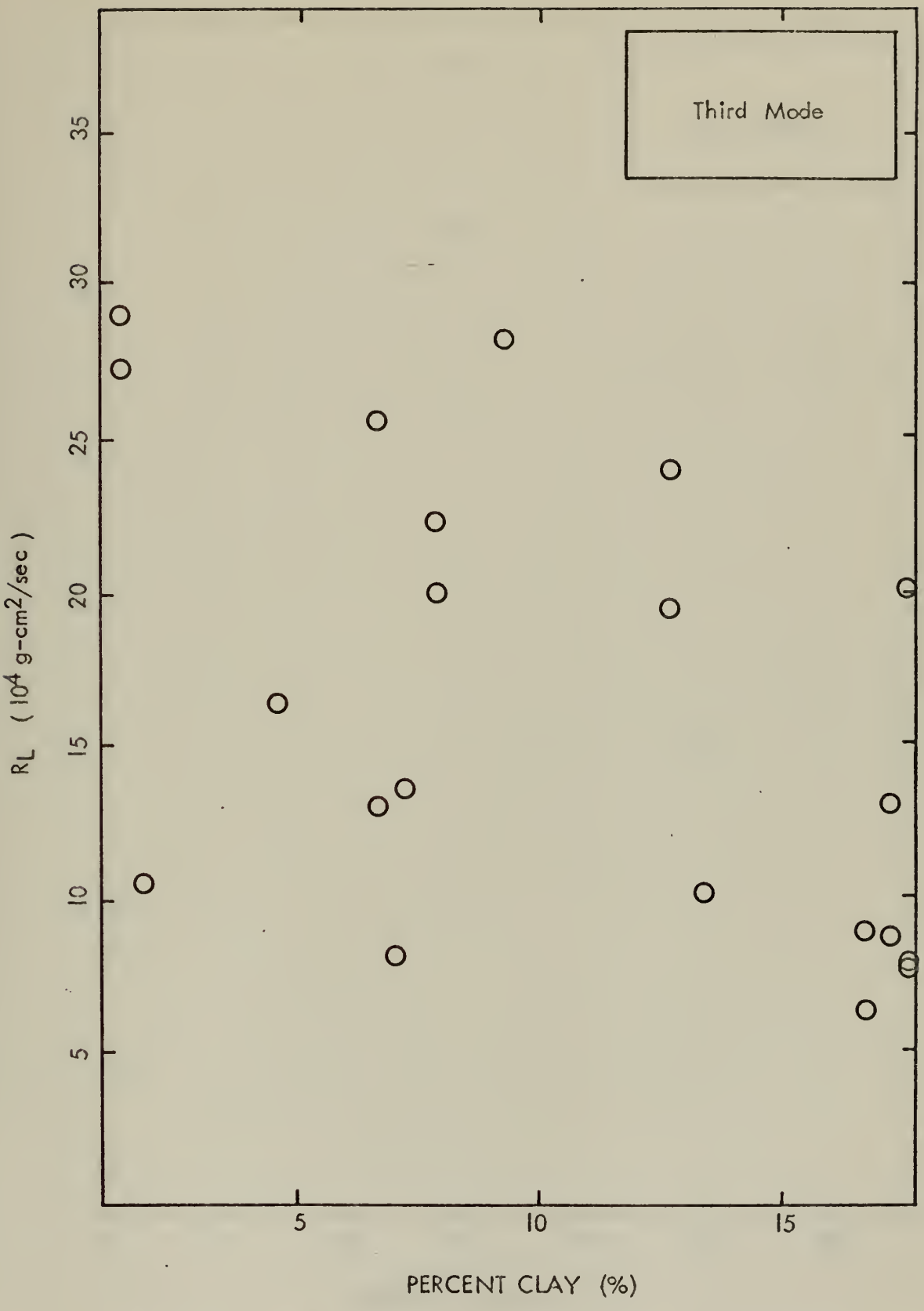

Figure 27. R_L as a Function of Percent Clay, Third Mode

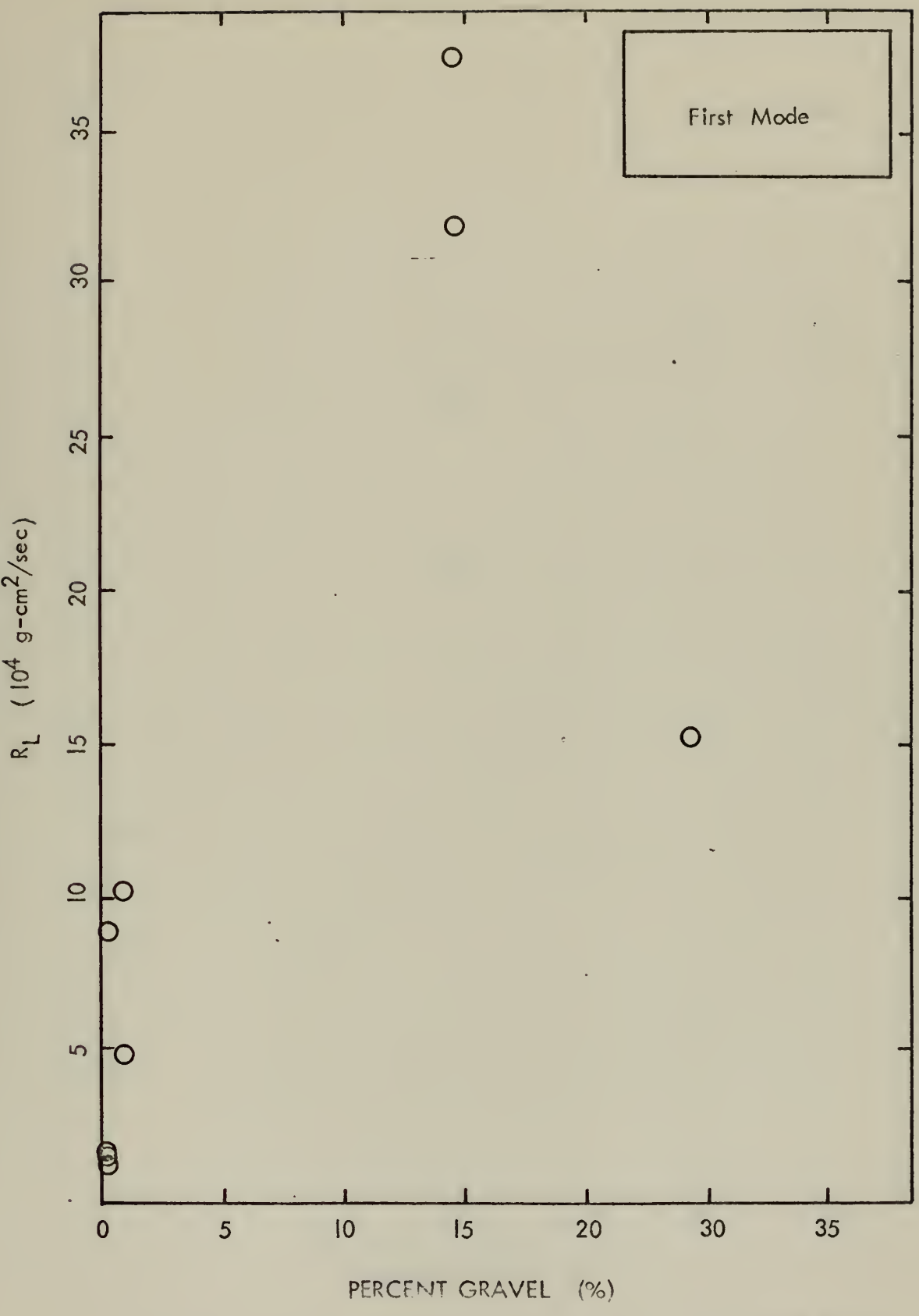

Figure 28. R_L as a Function of Percent Gravel, First Mode

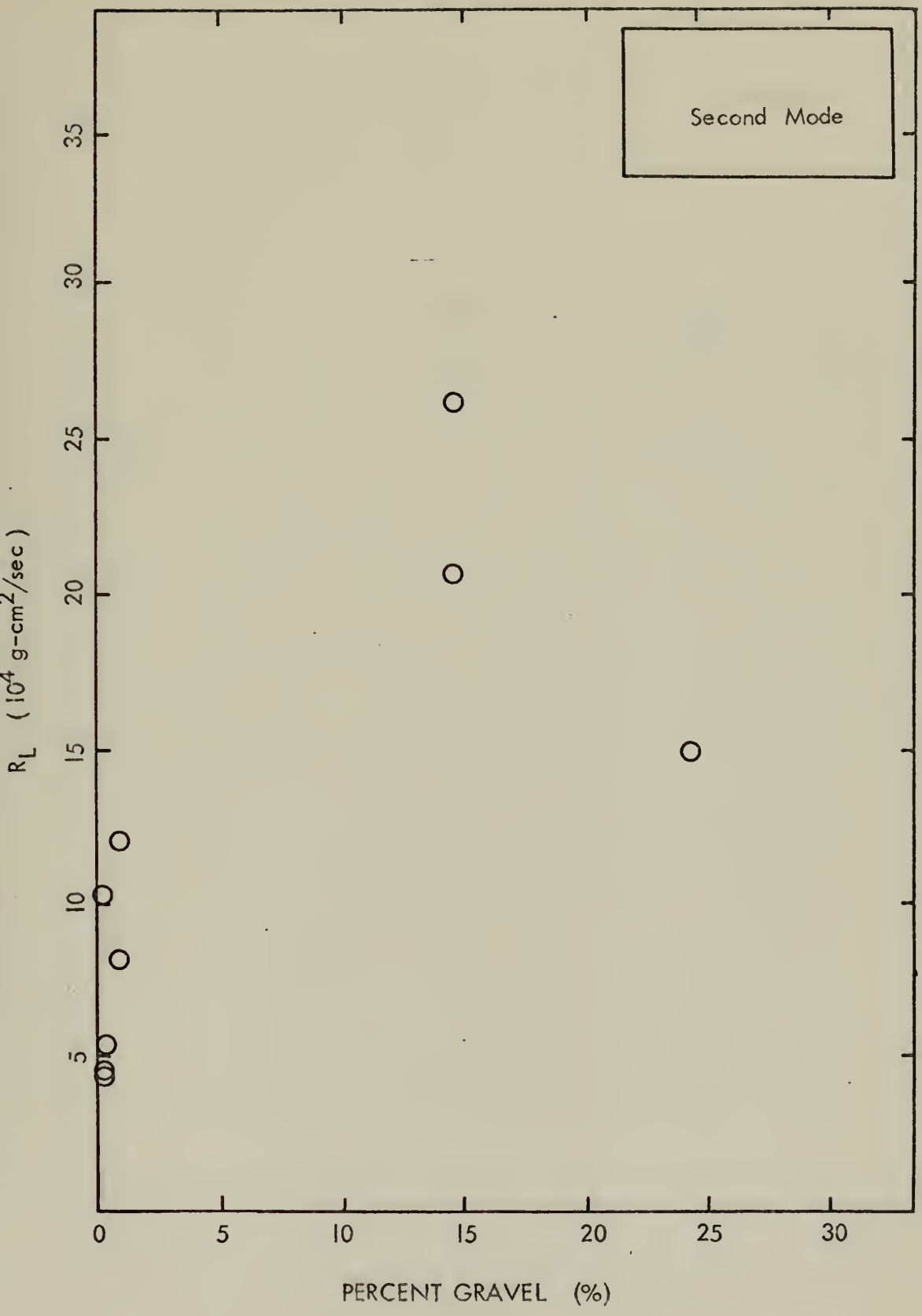

Figure 29. R_L as a Function of Percent Gravel, Second Mode

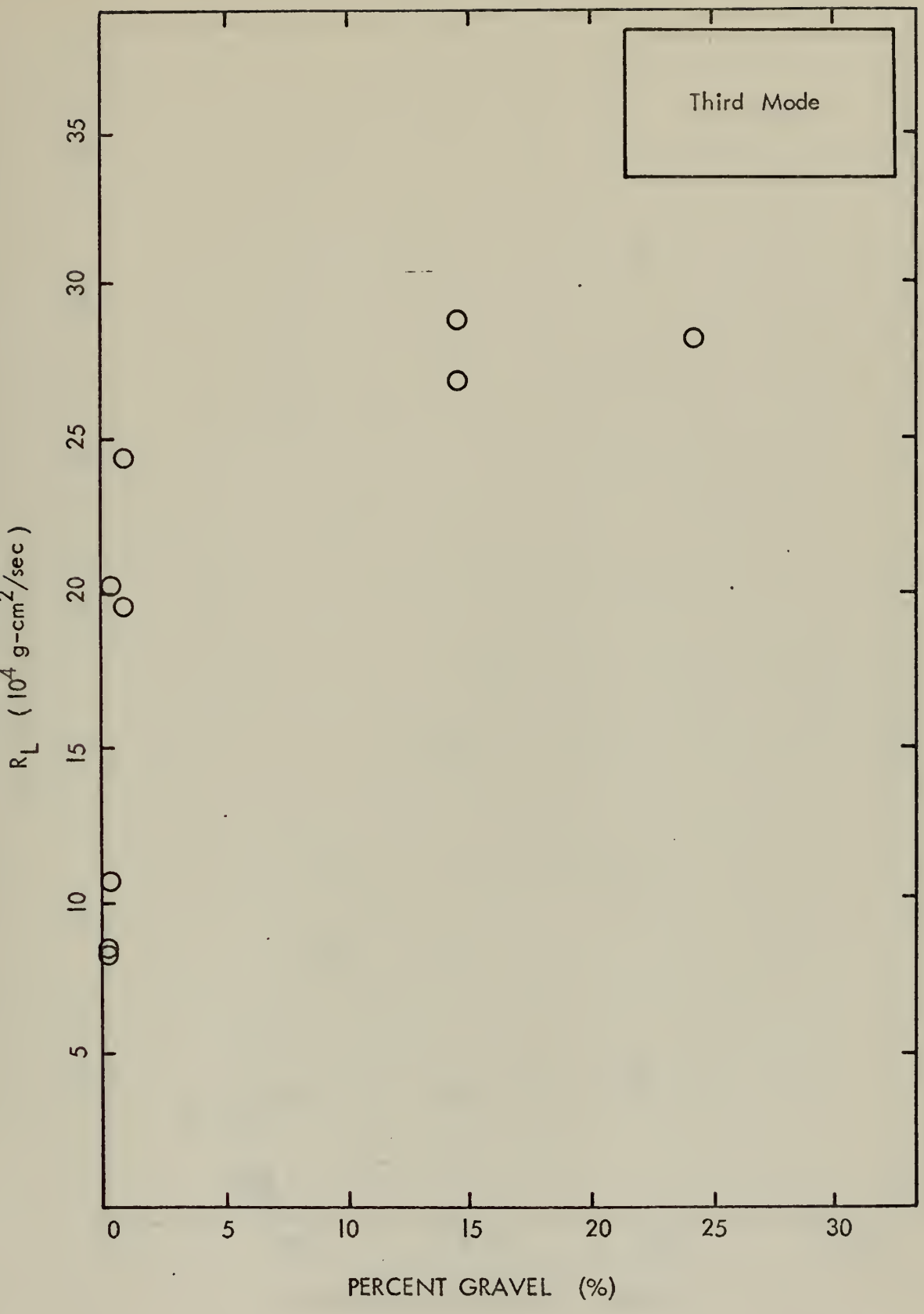

Figure 30. R_L as a Function of Percent Gravel, Third Mode

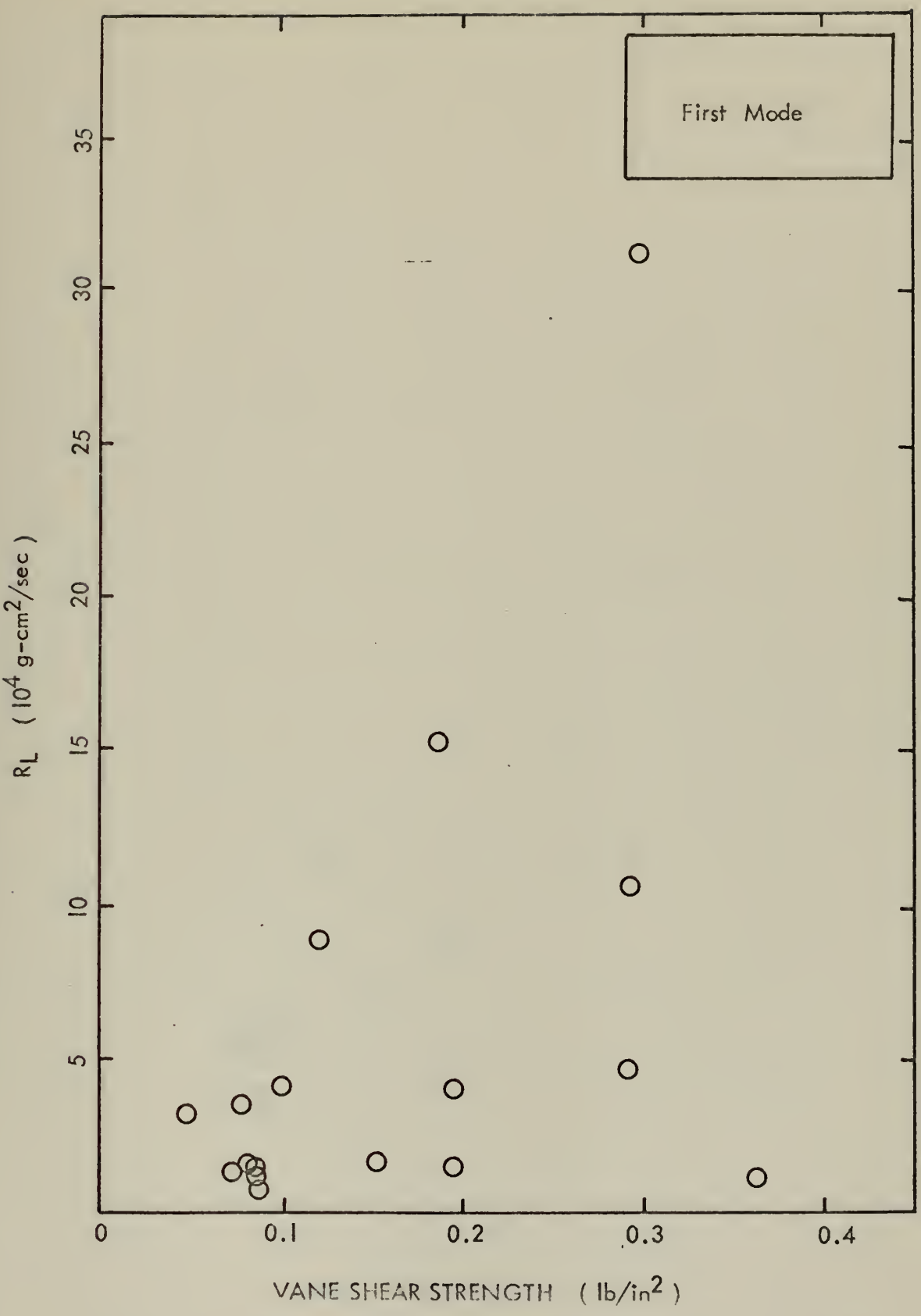

Figure 31. R_L as a Function of Vane Shear Strength, First Mode

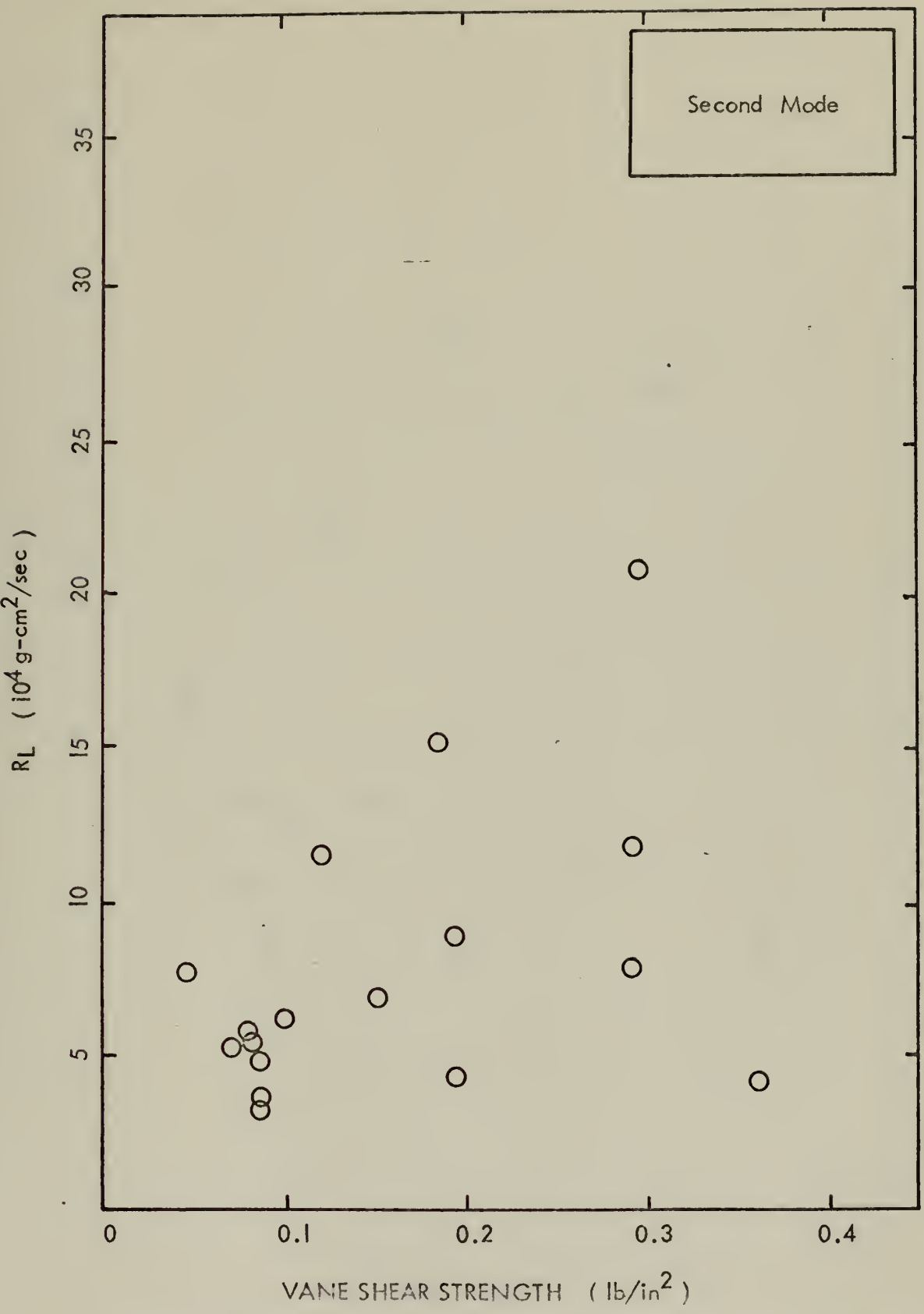

Figure 32. R_L as a Function of Vane Shear Strength, Second Mode

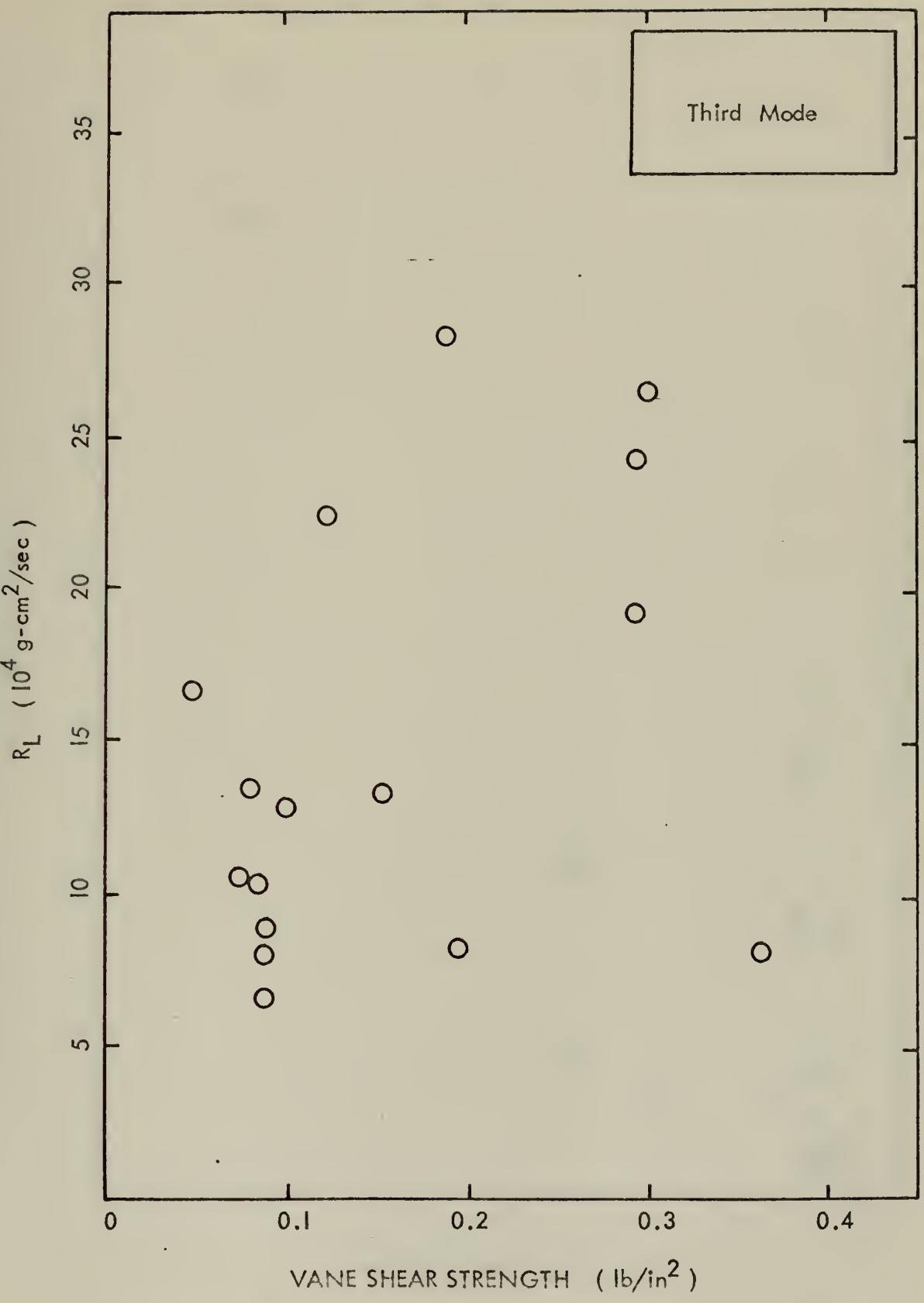

Figure 33. R_L as a Function of Vane Shear Strength, Third Mode

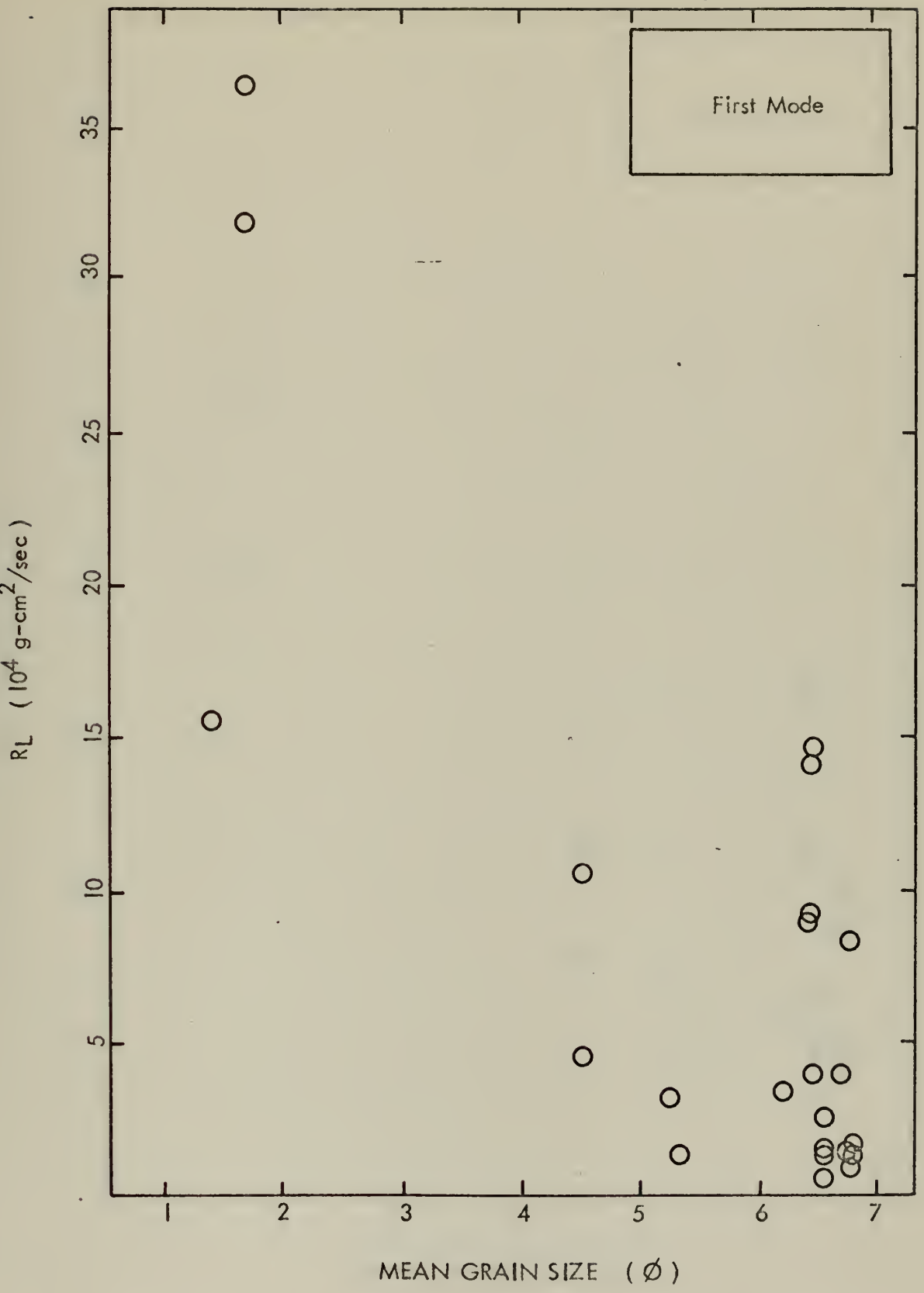

Figure 34. R_L as a Function of Mean Grain Size, First Mode

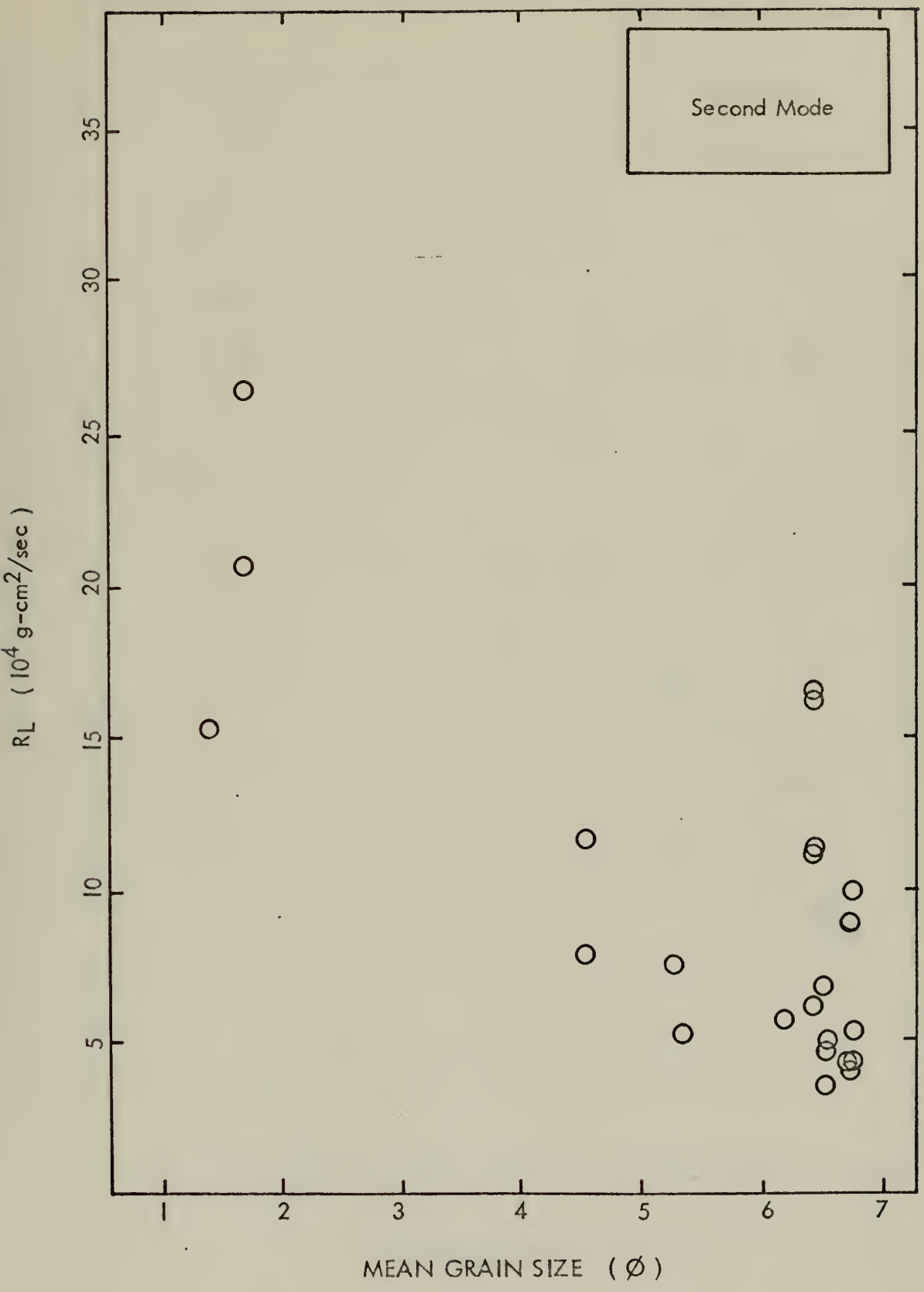

Figure 35. R_L as a Function of Mean Grain Size, Second Mode

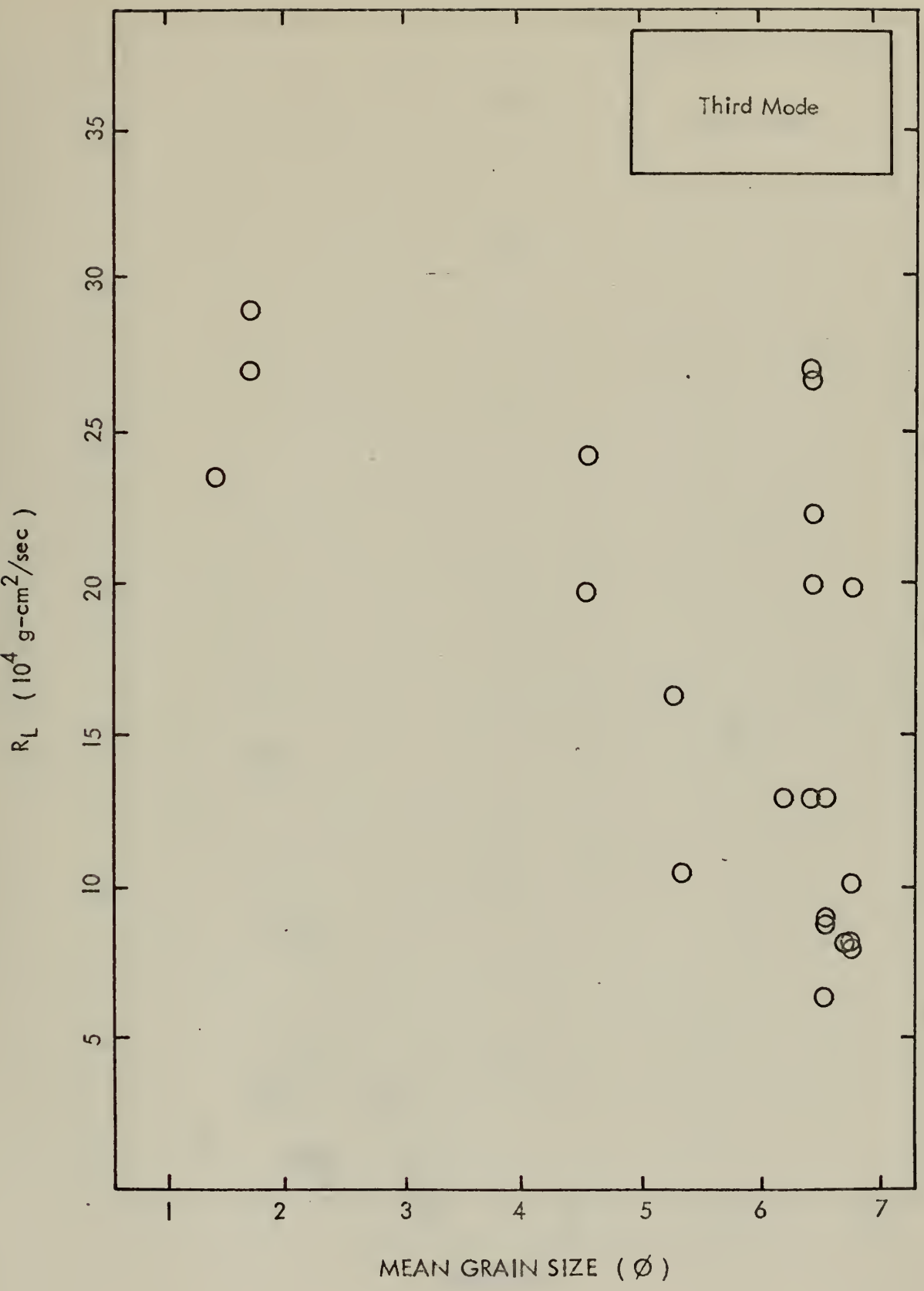

Figure 36. R_L as a Function of Mean Grain Size, Third Mode

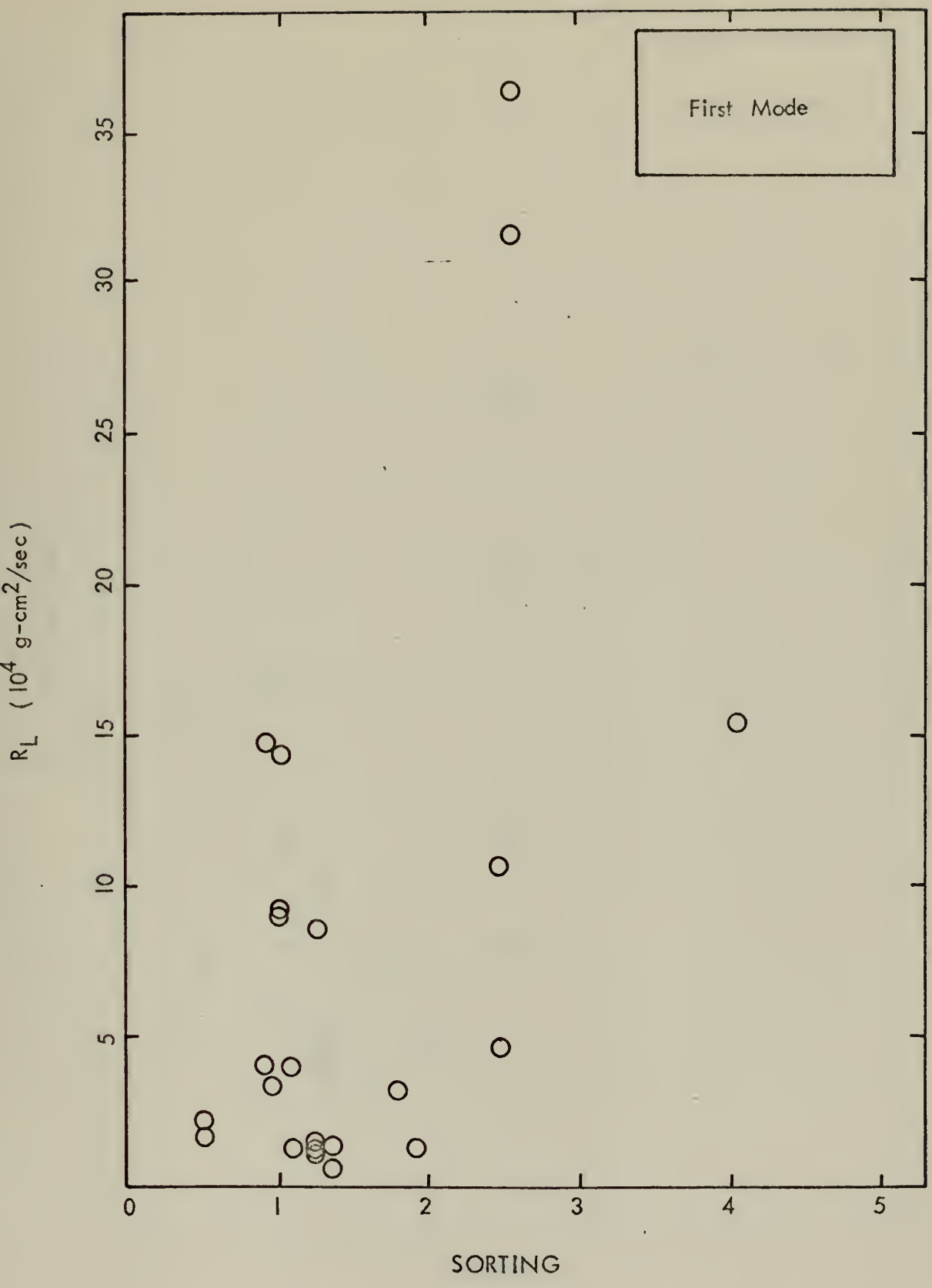

Figure 37. R_L as a Function of Sorting, First Mode

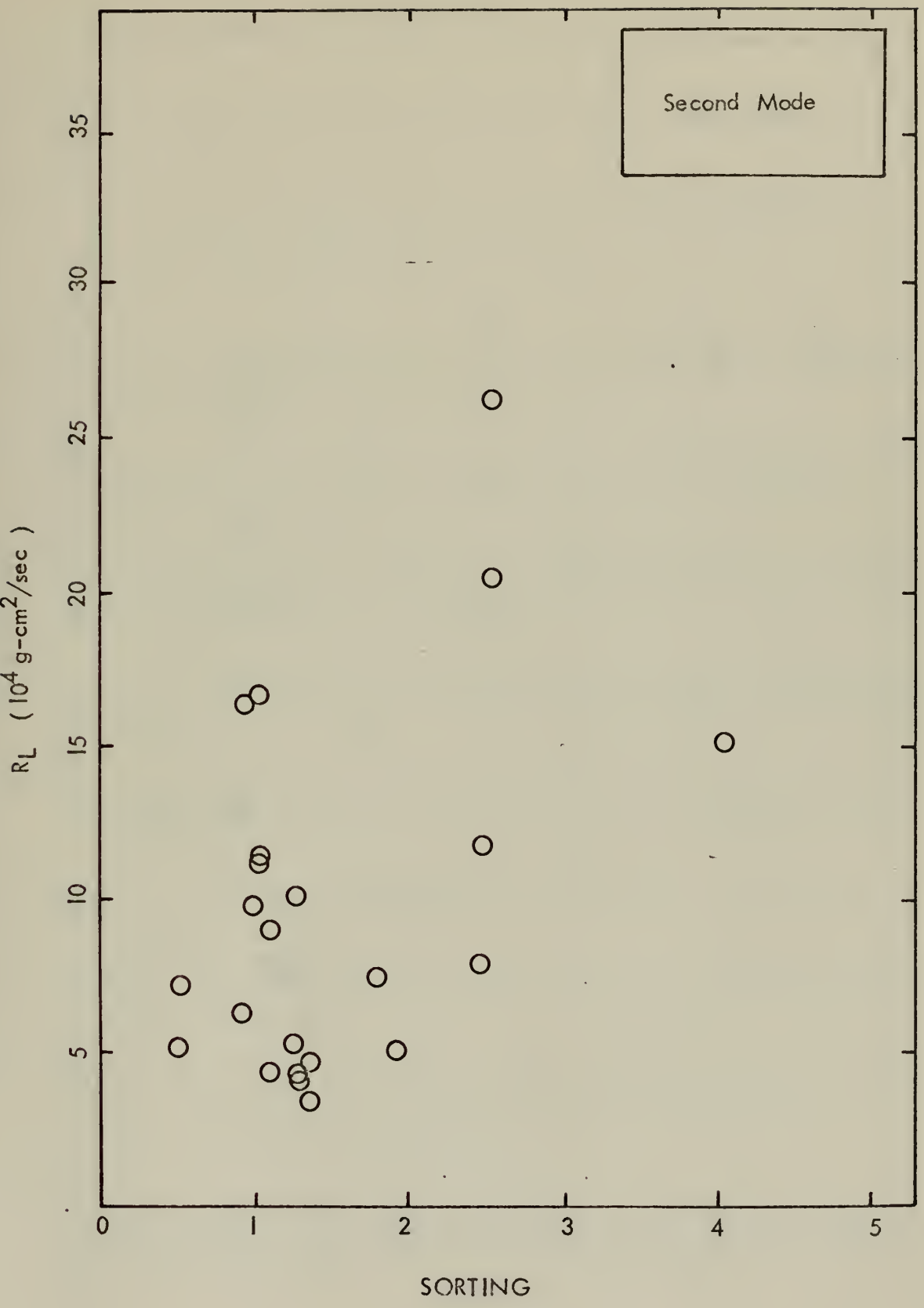

Figure 38. R_L as a Function of Sorting, Second Mode

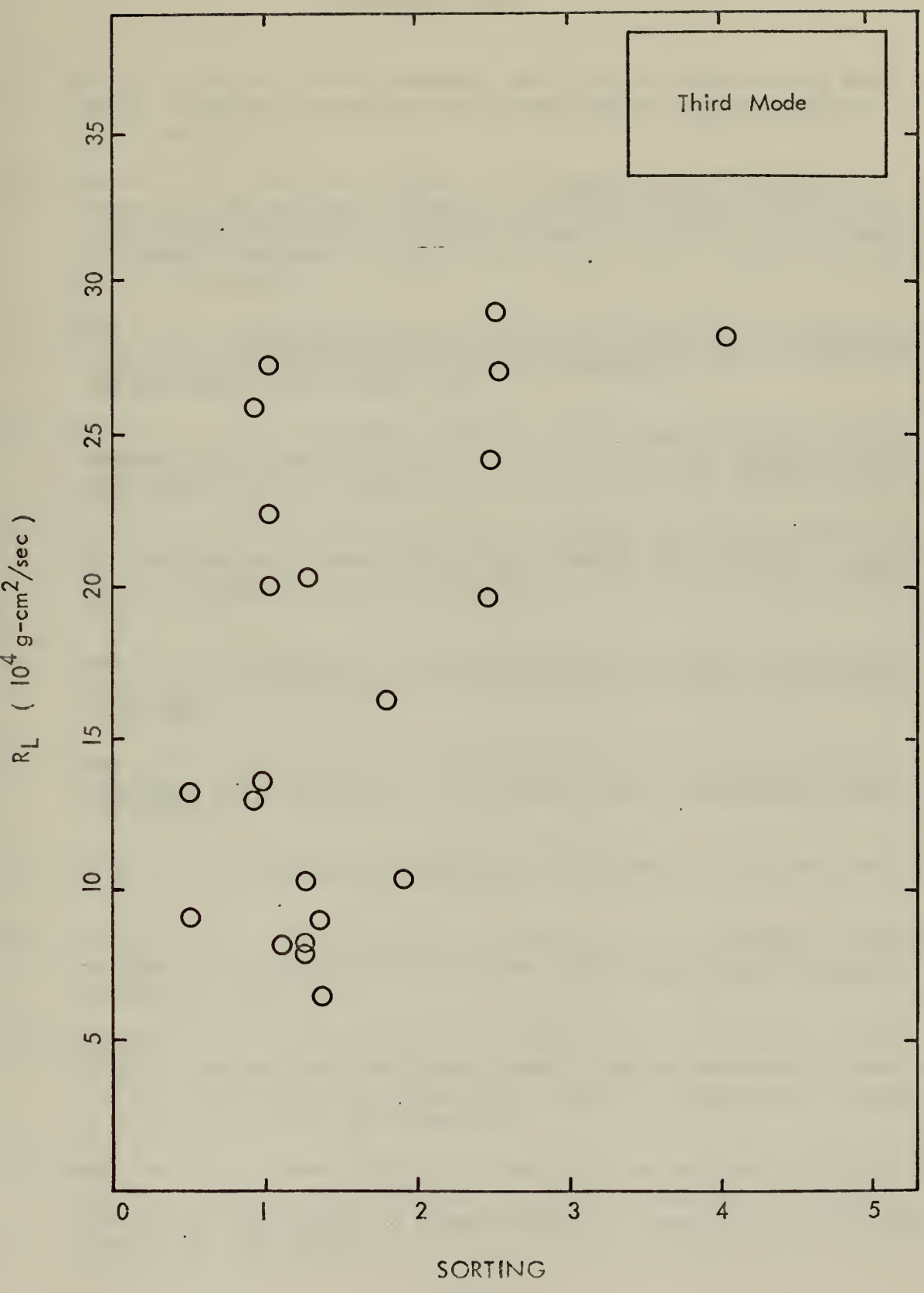

Figure 39. R_L as a Function of Sorting, Third Mode

REFERENCES CITED

1. Akal, T., The Relationship Between the Physical Properties of Underwater Sediments that Affect Bottom Reflection, Marine Geology, v. 13, 1972, pp 251-266.

2. Andrews, R. S. and O. B. Wilson, Jr., Measurement of Viscoelastic Properties of Sediments Using a Torsionally Vibrating Probe, paper presented at the Office of Naval Research Symposium on the Physics of Sound in Sediments, Austin, Texas, April 1973. (paper submitted for publication)

3. Beida, G. E., Measurement of the Viscoelastic and Related Mass-Physical Properties of Some Continental Terrace Sediments, M. S. Thesis, Naval Postgraduate School, 1970, 75p.

4. Bucker, H. P., J. A. Whitney, and D. L. Keir, Use of Stoneley Waves to Determine the Shear Velocities in Ocean Sediments, Journal of the Acoustical Society of America, v. 36, no. 5, 1964, pp 1595-1591.

5. Bucker, H. P., J. A. Whitney, G. S. Yee and R. R. Gardner, Reflection of Low-Frequency Sonar Signals from a Smooth Ocean Bottom, Journal of the Acoustical Society of America, v. 37, no. 6, 1965, pp 1037-1051.

6. Cepek, R. J., Acoustical and Mass-Physical Properties of Deep Ocean Recent Marine Sediments, M. S. Thesis, Naval Postgraduate School, 1972, 83p.

7. Cohen, S. R., Measurement of the Viscoelastic Properties of Water Saturated Clay Sediments, M. S. Thesis, Naval Postgraduate School, 1968, 57p.

8. Ferry, J. D., Viscoelastic Properties of Polymers, Wiley and Sons, Inc., 1970, 617p.

9. Gallagher, J. J. and V. A. Nacci, Investigations of Sediment Properties in Sonar Bottom Reflectivity Studies, Underwater Sound Laboratory Report No. 944, 1968.

10. Hamilton, E. L., H. P. Bucker, D. L. Keir, and J. A. Whitney, Velocities of Compressional and Shear Waves in Marine Sediments Determined In Situ from a Research Submersible, Journal of Geophysical Research, v. 75, no. 20, 1970, pp 4039-4049.

11. Hamilton, E. L., Sound Velocity, Elasticity and Related Properties of Marine Sediments, North Pacific, Part II; Elasticity and Elastic Constants, Naval Undersea Research and Development Center Technical Report No. 144, 1969.

12. Hutchins, J. R., Investigations of the Viscoelastic Properties of a Water Saturated Sediment, M. S. Thesis, Naval Postgraduate School, 1967, 30p.

13. Lasswell, J. B., A Comparison of Two Methods for Measuring Rigidity of Saturated Marine Sediments, M. S. Thesis, Naval Postgraduate School, 1970, 65p.

14. Mason, W. P., Measurements of the Viscosity and Shear Elasticity of Liquids by Means of a Torsionally Vibrating Crystal, Transactions of the A. S. M. E., May 1947, pp 359-370.

15. McSkimin, H. J., Measurements of Dynamic Shear Viscosity and Stiffness of Viscous Liquids by Means of Traveling Torsional Waves, The Journal of the Acoustical Society of America, v. 24, no. 4, 1952, pp 355-365.

16. Morgan, J. H., II, Design of an Instrument to Measure the Shear Modulus of Soft Sediments, M. S. Thesis, Naval Postgraduate School, 1972, 42p.

17. Walsh, W. F., Jr., The Use of Surface Wave Technique for Verification of Dynamic Rigidity Measurements in a Kaolinite-Water Artificial Sediment, M. S. Thesis, Naval Postgraduate School, 1971, 42p.

18. White, J. E., Seismic Waves: Radiation, Transmission, and Attenuation, McGraw-Hill Book Co., 1965, pp 302.

INITIAL DISTRIBUTION LIST

		No. Copies
1.	Defense Documentation Center Cameron Station Alexandria, Virginia 22314	2
2.	Library, Code 0212 Naval Postgraduate School Monterey, California 93940	2
3.	Professor O. B. Wilson, Jr., Code 61Wl Department of Physics Naval Postgraduate School Monterey, California 93940	5
4.	Professor R. S. Andrews, Code 58Ad Department of Oceanography Naval Postgraduate School Monterey, California 93940	5
5.	Department of Oceanography, Code 58 Naval Postgraduate School Monterey, California 93940	3
6.	Office of Naval Research Code 480D Arlington, Virginia 22217	1
7.	Oceanographer of the Navy Hoffman Building No. 2 2461 Eisenhower Avenue Alexandria, Virginia 22314	1
8.	Dr. William R. Bryant Texas A&M University Department of Oceanography College Station, Texas 77843	1
9.	Dr. Davis A. Fahlquist Texas A&M University Department of Geophysics College Station, Texas 77843	1
10.	Dr. E. L. Hamilton Naval Undersea Research and Development Center San Diego, California 92152	1
11.	LT S. B. Kramer, USN 3 Prairie Avenue Newport, R.I. 02840	1

		No. Copies
12.	Dr. Robert E. Stevenson Scientific Liaison Office Scripps Institution of Oceanography LaJolla, California 92037	1
13.	Mr. Homa Lee Naval Civil Engineering Laboratory Port Hueneume, California 93041	1
14.	Library U. S. Naval Oceanographic Office Washington, D. C. 20390	1
15.	Director of Defense Research and Engineering Office of the Secretary of Defense Washington, D.C. 20301 ATTN: Office, Assistant Director (Research)	1
16	Office of Naval Research Arlington, Virginia 22217	
	ATTN: (Code 460)*	1
	ATTN: (Code 102-OS)	1
	Cognizant ONR Branch Office	1
17	Director Naval Research Laboratory Washington, D.C. 20390	
	ATTN: Library, Code 2029 (ONRL)	6
	ATTN: Library, Code 2620	6
18	Commander Naval Oceanographic Office Washington, D.C. 20390	
	ATTN: Code 1640	1
	ATTN: Code 70	1
19	NODC/NOAA Rockville, MD 20882	1

SECURITY CLASSIFICATION OF THIS PAGE (When Data Entered)

REPORT DOCUMENTATION PAGE		READ INSTRUCTIONS BEFORE COMPLETING FORM
1. REPORT NUMBER	2. GOVT ACCESSION NO.	3. RECIPIENT'S CATALOG NUMBER
4. TITLE (and Subtitle) Measurement of Viscoelastic Properties of Some Recent Marine Sediments by a Torsionally Oscillating Cylinder Method		5. TYPE OF REPORT & PERIOD COVERED Master's Thesis: September 1973 6. PERFORMING ORG. REPORT NUMBER
7. AUTHOR(s) Steven Barker Kramer		8. CONTRACT OR GRANT NUMBER(s)
9. PERFORMING ORGANIZATION NAME AND ADDRESS Naval Postgraduate School Monterey, California 93940		10. PROGRAM ELEMENT, PROJECT, TASK AREA & WORK UNIT NUMBERS
11. CONTROLLING OFFICE NAME AND ADDRESS Naval Postgraduate School Monterey, California 93940		12. REPORT DATE September 1973 13. NUMBER OF PAGES 84
14. MONITORING AGENCY NAME & ADDRESS(if different from Controlling Office) Naval Postgraduate School Monterey, California 93940		15. SECURITY CLASS. (of this report) Unclassified 15a. DECLASSIFICATION/DOWNGRADING SCHEDULE

16. DISTRIBUTION STATEMENT (of this Report)

Approved for public release; distribution unlimited.

17. DISTRIBUTION STATEMENT (of the abstract entered in Block 20, if different from Report)

18. SUPPLEMENTARY NOTES

19. KEY WORDS (Continue on reverse side if necessary and identify by block number)

Marine Sediments
Properties Marine Sediments
Acoustic Reflection Coefficient
Shear Modulus Sediments
Dynamic Rigidity Sediments

20. ABSTRACT (Continue on reverse side if necessary and identify by block number)

A torsionally oscillating cylindrical probe method, operating in the frequency range of 0.8 to 3.3 kHz was employed for measuring the viscoelastic properties of 13 marine samples collected by Shipek grab from shallow water regions of Monterey Bay, California. Other mass physical properties such as wet density, porosity, sound speed, sand-silt-clay-gravel percentages, mean grain size and sorting were also measured. Limited precision of impedance

DD FORM 1 JAN 73 1473 EDITION OF 1 NOV 65 IS OBSOLETE
S/N 0102-014-6601 |
(Page 1)

SECURITY CLASSIFICATION OF THIS PAGE (When Data Entered)

Item 20 (Continued)

measurements permitted only the determination of the mechanical resistance due to the probe contact with the sediment. The observed values for various sediments ranged up to a value 65 times the lowest value. Correlations between mechanical resistance and mass physical properties are studied by graphical means with results indicating that water content of sediments is a determining factor in the mechanical resistance of a sediment. A dependence of mechanical resistance upon frequency is observed.

Thesis
K8485 Kramer
c.1

146109

Measurement of viscoelastic properties of some recent marine sediments by a torsionally oscillating cylinder method.

Thesis
K8485 Kramer
c.1

146109

Measurement of viscoelastic properties of some recent marine sediments by a torsionally oscillating cylinder method.

thesK8485
Measurement of viscoelastic properties o
3 2768 002 11516 4
DUDLEY KNOX LIBRARY